Implementation of an all-electron GW Approximation using the Projector Augmented Wave method: I. Formulation and application to the electronic structure of semiconductors

B. Arnaud and M. Alouani

Institut de Physique et de Chimie des Matériaux de Strasbourg (IPCMS), 23 rue du Loess,67037

Strasbourg, France

(February 8, 2020)

Abstract

We have implemented the so called GW approximation (GWA) based on an all-electron full-potential Projector Augmented Wave (PAW) method. For the screening of the Coulomb interaction W we tested three different plasmon-pole dielectric function models, and showed that the accuracy of the quasiparticle energies is not sensitive to the the details of these models. We have then applied this new method to compute the quasiparticle band structure of some small, medium and large-band-gap semiconductors: Si, GaAs, AlAs, InP, SiMg₂, C and (insulator) LiCl. A special attention was devoted to the convergence of the self-energy with respect to both the \mathbf{k} -points in the Brillouin zone and to the number of reciprocal space \mathbf{G} -vectors. The most important result is that although the all-electron GWA improves considerably the quasiparticle band structure of semiconductors, it does not always provide the correct energy band gaps as originally claimed by GWA pseudopotential type of calculations. We argue that the decoupling between the valence and core electrons is a problem, and is some what hidden in a pseudopotential type of

approach.

 $71.20.\mathrm{Ap},\,71.15.\mathrm{Mb},\,71.20.\mathrm{-b},\,71.20.\mathrm{Nr}$

I. INTRODUCTION

In the last few years, with the increase of computer power, many researchers have tried to unify two major but different approaches to the computation of electronic properties of materials: (1) The local density approximation (LDA) to the Kohn-Sham equations¹ where the correlation effects are included in an average way through the use of the parameterized local exchange-correlation potential.² (2) Many-body models based on simplified and parameterized Hamiltonians omitting much of the subtlety of the chemical bonding but handling the correlation effects effectively. The aim of the unification being to provide a good description of the quasi-particles properties in *real* solids without omitting either the subtlety of chemical bonding or the correlated nature of the electrons.³⁻²¹

That LDA is inadequate has been known for example in the case of semiconductors: the LDA band gaps are at least 50% smaller than experimental values. It was shown by Perdew and Levy²² and Sham and Schlüter²³ that the difference between the highest occupied and lowest unoccupied state of the density functional theory (DFT) eigenvalues is not the true quasiparticle band gap, but differs from it by Δ , the discontinuity in the exchange-correlation potential when an electron is added to the system. Later, it was shown that quasiparticle calculation based on the the GW approximation (GWA) of Hedin^{3,4} produced band gaps which were in good agreement with experiment.⁵⁻¹⁹ This development in the theoretical study of the electronic structure of solids is the inclusion of many-body effects in the calculation, principally, through the computation of the quasiparticle self-energy and the results are an adjustment of the energy splittings obtained within the local density approximation.¹

After this initial success the GWA has been extensively used to study other properties of different type of materials: (1) The band-width narrowing in alkali-metals, and their clusters.^{24,25} (2) The surfaces states of semiconductors, i.e., improving band gaps of surface states,²⁶ looking for dimer buckling in Si surfaces.²⁷ (3) The effects of correlation on the valence off-set between different bulk semiconductors.²⁸ (4) The character of the band gaps

of superlattices and anisotropy of optical matrix elements.²⁹ (5) The orientational disorder and photoemission spectra of solid C_{60} .¹⁶ (6) The electronic properties of elemental Ni and its energy loss spectra.¹⁵ (7) The quasiparticle properties of atoms using various GWA.³⁰ (8) The Schottky barrier between a metal and a semiconductor.³¹ (9) The inclusion of excitonic effects in the calculation of the dielectric function of semiconductors^{32–34}. All these different studies in a very short time established the GWA as a good 'first-principles' method for computations of quasiparticle properties of real materials.

In most of these studies the plane wave expansion of the LDA pseudopotential basisset is used, which makes an analysis in terms of chemically relevant orbitals difficult. An additional difficulty with doing the GWA to the self-energy in a plane wave basis set is that the computational effort for systems with localized electrons is enormous since the plane wave expansion of the wave function becomes a real problem especially for systems of localized electrons or low dimensional materials.

In this paper, we propose a new implementation of the GWA based on an all-electron method using the recently developed all-electron projector augmented wave (PAW) method. To Our constructed ab-initio method of quasiparticles is then based on the framework of the LDA theory in conjunction with the PAW method. The knowledge of the one-electron Green function provided by the PAW method allows us to construct the quasiparticle self-energy within the GWA, in which the dynamical screening of the electron-electron interaction arises from a plasmon model dielectric function 10,13,36 for which the parameters are adjusted to the dielectric function calculated in the random-phase-approximation (RPA). The full calculation of systems of many atoms in the unit cell is prohibitive on sequential computers, so we had to parallelize our numerical code so that the calculations become feasible on scalable parallel architectures.

Our paper is organized as follows: In the fist part we introduce the projector augmented wave method which is used to solve the Kohn-Sham equations and provides the one-electron Green's function and the RPA dielectric function which are then used to compute the self-energy. We then describe our GW implementation based on the PAW method and show

the difficulties, traps, encountered when implementing an all-electron GWA. In particular, we mention the difficulty related to the decoupling of the core and valence electrons. We discuss also in details the use of symmetry to reduce the computational time of the self-energy and the dielectric function, as well as the parallelization of our numerical code. In the third section we apply our method to determine the electronic structure of two distinct semiconductor groups: some small and medium-band-gap semiconductors: Si, GaAs, AlAs, InP, Mg₂Si and some large-band-gap semiconductors (insulator): C, and (LiCl). We then compare our results with available GWA calculations and experiments.

II. METHOD OF CALCULATION

A. A brief introduction of the PAW method

In the density functional theory implemented in the framework of the LDA¹, an electronic structure calculation requires the solution of Kohn-Sham type of equations in a self consistent way. The computation of material's band structure consists in finding the Bloch wave functions $\Psi_{n\mathbf{k}}(r)$, where n and \mathbf{k} denote a band index and a wave vector in the Brillouin zone, respectively. In the projector augmented plane wave (PAW) formalism,³⁵ all calculations are performed on a smooth "pseudo" wave function $\tilde{\Psi}_{n\mathbf{k}}(r)$ which is expressed as a linear combination of plane waves. The passage from the smooth pseudo-wave function to the all-electron wave function exhibiting the correct nodal behavior in the augmentation regions (spheres centered on each atom) is achieved by defining three atomic type of functions in each augmentation region: (1) The all-electron basis functions $\Phi_i^a(r)$, (2) The 'pseudo' basis functions $\tilde{\Phi}_i^a(r)$, (3) The projector functions $\tilde{p}_i^a(r)$. Here $i = l_i, m_i, n_i$ where l_i and m_i denote the orbital and magnetic quantum numbers, respectively. The index n_i is introduced to leave the opportunity of choosing more than one function for each angular momentum channel (l_i, m_i) . These functions are defined so that:

$$\tilde{\Phi}_i^a(r) = \Phi_i^a(r) \qquad \text{for } r \ge r_c^a \tag{1}$$

where r_c^a are the radii of non-overlapping spheres centered at each atomic site a. The projector functions vanish for $r \geq r_c^a$ and satisfy the orthogonality property:

$$\langle \tilde{p}_i^a | \tilde{\Phi}_j^a \rangle = \delta_{ij} \tag{2}$$

Using these functions, the all-electron wave function $\Psi_{nk}(r)$ can be deduced from the 'pseudo' wave function $\tilde{\Psi}_{nk}(\mathbf{r})$ according to the relation $\Psi_{nk}(\mathbf{r}) = \tilde{\Psi}_{nk}(\mathbf{r}) + \Psi_{nk}^1(\mathbf{r}) - \tilde{\Psi}_{nk}^1(\mathbf{r})$ with

$$\Psi_{n\mathbf{k}}^{1}(\mathbf{r}) - \tilde{\Psi}_{n\mathbf{k}}^{1}(\mathbf{r}) = \sum_{a,i} \left[\Phi_{i}^{a}(\mathbf{r} - \mathbf{R}^{\mathbf{a}}) - \tilde{\Phi}_{i}^{a}(\mathbf{r} - \mathbf{R}^{\mathbf{a}}) \right] \langle \tilde{p}_{i}^{a} | \tilde{\Psi}_{n\mathbf{k}} \rangle$$
(3)

where $\mathbf{R}^{\mathbf{a}}$ denotes the atomic position of the atom a in the unit cell. It is useful to point out the fact that $\Psi_{n\mathbf{k}}^1 - \tilde{\Psi}_{n\mathbf{k}}^1$ vanishes in the interstitial region and defines the quantity necessary to describe the true wave function in the augmentation regions while $\tilde{\Psi}_{n\mathbf{k}}$ describes the true wave function in the interstitial region.

The PAW formalism is designed to easily calculate the expectation value of local or semilocal observables. For example the expectation value of an operator $A(\mathbf{r})$ between two Bloch wave functions $\Psi_{n\mathbf{k}}$ and $\Psi_{m\mathbf{k}}$ can be calculated as a sum of three contributions:

$$A_{n\mathbf{k},m\mathbf{k}} = \langle \Psi_{n\mathbf{k}} | A | \Psi_{m\mathbf{k}} \rangle = \tilde{A}_{n\mathbf{k},m\mathbf{k}} + A_{n\mathbf{k},m\mathbf{k}}^1 - \tilde{A}_{n\mathbf{k},m\mathbf{k}}^1$$
 (4)

where

$$\tilde{A}_{n\mathbf{k},m\mathbf{k}} = \langle \tilde{\Psi}_{n\mathbf{k}} | A | \tilde{\Psi}_{m\mathbf{k}} \rangle \tag{5}$$

This contribution is evaluated in the plane wave basis set. The last two contributions

$$A_{n\mathbf{k},m\mathbf{k}}^{1} = \sum_{i,j,a} \langle \tilde{\Psi}_{n\mathbf{k}} | \tilde{p}_{i}^{a} \rangle \langle \Phi_{i}^{a} | A | \Phi_{j}^{a} \rangle \langle \tilde{p}_{j}^{a} | \tilde{\Psi}_{m\mathbf{k}} \rangle$$
 (6)

and

$$\tilde{A}_{n\mathbf{k},m\mathbf{k}}^{1} = \sum_{i,j,a} \langle \tilde{\Psi}_{n\mathbf{k}} | \tilde{p}_{i}^{a} \rangle \langle \tilde{\Phi}_{i}^{a} | A | \tilde{\Phi}_{j}^{a} \rangle \langle \tilde{p}_{j}^{a} | \tilde{\Psi}_{m\mathbf{k}} \rangle$$

$$(7)$$

are evaluated in the augmentation regions.

Blöchl³⁵ managed to decompose the total valence energy into three contributions in complete analogy with the decomposition of the expectation value of an operator

$$E = \tilde{E} + E^1 - \tilde{E}^1 \tag{8}$$

where E includes the kinetic energy of the valence electrons, the interaction energy with the nuclei having atomic number Z^a and with the core electrons, which are described in the frozen core approximation, the Hartree energy and the exchange correlation energy of the valence electrons.

Minimizing the total energy with respect to the $\tilde{\Psi}_{n\mathbf{k}}$ (variationnal principle) leads to a generalized eigenvalue problem which is solved in a self-consistent way, giving the pseudo wave functions $\tilde{\Psi}_{n\mathbf{k}}$ from which the all-electron wave functions $\Psi_{n\mathbf{k}}$ are easily deduced by means of equation 3.

B. The GW approximation

1. Quasiparticle calculation in the GW approximation

Solving the Kohn-Sham equations, where the exchange-correlation effects are included in a mean way in an exchange-correlation potential $V_{xc}^{LDA}(r)$ yields to eigenvalues which can not be assimilated to the excitation energies of the solids. Indeed, there isn't any Koopman's theorem for the Kohn-Sham theory and these eigenvalues only have meaning as Lagrange parameters. The Green's function theory is a good tool for properly describing the excitation energies. In the quasiparticle approximation, we can find the excitation energies of the system by solving a quasiparticle equation

$$(T + V_{ext} + V_h)\psi_{\mathbf{k}n}(\mathbf{r}) + \int d^3r' \Sigma(\mathbf{r}, \mathbf{r}', E_n(\mathbf{k}))\psi_{\mathbf{k}n}(\mathbf{r}') = E_n(\mathbf{k})\psi_{\mathbf{k}n}(\mathbf{r})$$
(9)

instead of locating the poles of the Green's function. Here, T is the kinetic energy operator $(-\frac{1}{2}\nabla^2)$ in atomic units), V_{ext} is the external (ionic) potential, V_h is the Hartree potential due to the average Coulomb repulsion of the electrons and Σ is the self-energy operator which summarizes the many-body effects. Σ is in general a non local, energy-dependent, non-Hermitian operator. The non-Hermitian part of Σ gives rise to complex eigenvalues $E_n(\mathbf{k})$.

The real part of the eigenvalue is associated with the energy of the quasiparticle while the imaginary part is related to the inverse of the lifetime of the quasiparticle. Fortunately, the imaginary part of the eigenvalue, which can be attributed to the possibility for the quasiparticle to lower its energy via particle-hole formations (the decay of the quasiparticle via emission or absorption of plasmons is not effective near the Fermi level), becomes small near the Fermi level because of the restriction of the phase space for these processes. This is known as Pauli blocking. So, the quasiparticle concept is effective near the Fermi Level.

The similitude between the quasiparticle equation and the familiar self-consistent field equation in the Kohn-Sham formulation of the density-functional theory

$$(T + V_{ext} + V_h + V_{xc})\Psi_{\mathbf{k}n}(\mathbf{r}) = \epsilon_n(\mathbf{k})\Psi_{\mathbf{k}n}(\mathbf{r})$$
(10)

is striking if we set $\Sigma^{LDA} = \delta(E)\delta(\mathbf{r}, \mathbf{r}')V_{xc}(\mathbf{r})$ in the quasiparticle equation. So the Kohn-Sham equation can be regarded as an approximation to the quasiparticle equation where the self-energy is approximated by a local and energy-independent potential.

A more realistic, but relatively simple approximation to the self-energy, which takes into account both non-locality and dynamic correlations, known as the GW approximation (GWA), was initiated by Hedin^{3,4}. This approximation was originally derived from a many-body perturbation theory as the first term in the expansion of the self-energy in the screened interaction W. Within this scheme, the self-energy

$$\Sigma(\mathbf{r}, \mathbf{r}', \omega) = \frac{i}{2\pi} \int d\omega' G(\mathbf{r}, \mathbf{r}', \omega + \omega') e^{i\delta\omega'} W(\mathbf{r}, \mathbf{r}', \omega')$$
(11)

is approximated by a convolution with respect to the frequency variable of the Green's function with the screened interaction along the real axis. Here δ is a positive infinitesimal which ensures that only the poles of the Green's function associated to occupied states contribute to the integral, G is the best available Green's function and W is the best available screened Coulomb interaction. Accordingly, G is taken to be the Green's function built from LDA orbitals

$$G(\mathbf{r}, \mathbf{r}', \omega) = \lim_{\delta \to 0^{+}} \sum_{n\mathbf{k}} \frac{\Psi_{\mathbf{k}n}(\mathbf{r})\Psi_{\mathbf{k}n}^{*}(\mathbf{r}')}{\omega - \epsilon_{n}(\mathbf{k}) + i\delta sgn(\epsilon_{n}(\mathbf{k}) - \mu)}$$
(12)

where μ denotes the chemical potential, and where $\delta \to 0^+$ means δ being a positive infinitesimal number.

The dynamically screened interaction is defined by

$$W(\mathbf{r}, \mathbf{r}', \omega) = \int d\mathbf{r}'' \epsilon^{-1}(\mathbf{r}, \mathbf{r}'', \omega) v(\mathbf{r}'', \mathbf{r}')$$
(13)

where v denotes the bare Coulomb interaction and ϵ the dielectric function defined by

$$\epsilon(\mathbf{r}, \mathbf{r}', \omega) = \delta(\mathbf{r} - \mathbf{r}') - \int v(\mathbf{r}, \mathbf{r}'') P^{0}(\mathbf{r}'', \mathbf{r}', \omega) d\mathbf{r}''$$
(14)

where the irreducible polarisability P^0 is calculated within the RPA approximation (Bubble approximation)

$$P^{0}(\mathbf{r}, \mathbf{r}', \omega) = -\frac{i}{2\pi} \int d\omega' G(\mathbf{r}, \mathbf{r}', \omega) G(\mathbf{r}', \mathbf{r}, \omega' - \omega) e^{i\delta\omega'}$$
(15)

Using the LDA expression of the Green's function and integrating in the complex plane leads to the familiar expression of the irreducible polarisability

$$P^{0}(\mathbf{r}, \mathbf{r}', \omega) = \sum_{l\mathbf{k}, m\mathbf{k}'} \frac{[n_{l}(\mathbf{k}) - n_{m}(\mathbf{k}')]\Psi_{\mathbf{k}l}(\mathbf{r})\Psi_{\mathbf{k}l}^{*}(\mathbf{r}')\Psi_{\mathbf{k}'m}(\mathbf{r}')\Psi_{\mathbf{k}'m}^{*}(\mathbf{r}')}{\epsilon_{l}(\mathbf{k}) - \epsilon_{m}(\mathbf{k}') - \omega + i\delta[n_{l}(\mathbf{k}) - n_{m}(\mathbf{k}')]}$$
(16)

After having defined the different quantities, which enter the self-energy in the GW approximation, it is natural to look for the solution of the quasiparticle equation along the following line

$$\psi_{\mathbf{k}m}(r) = \sum_{n} \alpha_{mn}(\mathbf{k}) \Psi_{\mathbf{k}n}(r)$$
(17)

It has been shown by inspection that, $\alpha_{mn} \simeq \delta_{mn}$, which means that the quasiparticle Hamiltonian is virtually diagonal in the $\Psi_{\mathbf{k}n}$ basis for semiconductors such as Si⁵. A plausible argument for neglecting the non-diagonal part has been given recently by Hedin.³⁸ Since the quasiparticle wave functions $\psi_{\mathbf{k}m}$ are similar to the LDA wave functions $\Psi_{\mathbf{k}n}$ (the overlap between the quasiparticle wave function and the LDA wave function is about 99 %⁵), the numerical work is therefore considerably reduced. Indeed, using first order perturbation theory yields the following result:

$$E_n(\mathbf{k}) = \epsilon_n(\mathbf{k}) + \langle \Psi_{\mathbf{k}n} | \Sigma(\mathbf{r}, \mathbf{r}', E_n(\mathbf{k})) | \Psi_{\mathbf{k}n} \rangle - \langle \Psi_{\mathbf{k}n} | V_{xc}^{LDA}(\mathbf{r}) | \Psi_{\mathbf{k}n} \rangle$$
(18)

In principle, the solution to this equation should be obtained via an iterative method, but expanding Eq. (18) to first order in energy around $\epsilon_n(\mathbf{k})$ yields accurate numerical results. Then the quasiparticle energy can be obtained via

$$E_n(\mathbf{k}) - \epsilon_n(\mathbf{k}) = Z_{n\mathbf{k}}[\langle \Psi_{\mathbf{k}n} | \Sigma(\mathbf{r}, \mathbf{r}', \epsilon_n(\mathbf{k})) | \Psi_{\mathbf{k}n} \rangle - \langle \Psi_{\mathbf{k}n} | V_{xc}^{LDA}(r) | \Psi_{\mathbf{k}n} \rangle]$$
(19)

where the quasiparticle renormalization factor $Z_{n\mathbf{k}}$ is

$$Z_{n\mathbf{k}} = \left[1 - \langle \Psi_{\mathbf{k}n} | \frac{\partial}{\partial \omega} \Sigma(\mathbf{r}, \mathbf{r}', \epsilon_n(\mathbf{k})) | \Psi_{\mathbf{k}n} \rangle\right]^{-1}$$
(20)

Since $\frac{\partial}{\partial \omega} \Sigma < 0$, we have $0 < Z_{n\mathbf{k}} < 1$ with typical values of 0.8 for bands close to the band gap and for all materials considered here (see Table I). Values of $Z_{n\mathbf{k}}$ about 0.8 imply that we still have well-defined quasiparticles in the system but that 20 percents of the spectral weight is now distributed over a range of frequencies.

2. Calculating the matrix elements of Σ within the PAW formalism

As can be seen from Eq. (19), the central problem of this scheme consists in evaluating the diagonal matrix elements of the self-energy between LDA orbitals. The quantities which enter the self-energy are functions f of two locations \mathbf{r} and \mathbf{r}' . These functions have the following translational symmetry property $f(\mathbf{r} + \mathbf{R}, \mathbf{r}' + \mathbf{R}) = f(\mathbf{r}, \mathbf{r}')$ where R is a Bravais lattice vector. Then, we can fix the Fourier transform convention for such functions

$$f(\mathbf{r}, \mathbf{r}', \omega) = \frac{1}{\Omega} \sum_{\mathbf{q}, \mathbf{G}, \mathbf{G}'} e^{i(\mathbf{q} + \mathbf{G}) \cdot r} f_{\mathbf{G}\mathbf{G}'}(\mathbf{q}, \omega) e^{-i(\mathbf{q} + \mathbf{G}') \cdot \mathbf{r}'}$$
(21)

where \mathbf{q} is a wave vector in the first Brillouin zone, \mathbf{G} a reciprocal lattice vector and Ω the crystal volume.

In the plane wave basis, the dielectric function can be defined as

$$\epsilon_{\mathbf{GG'}}(\mathbf{q},\omega) = \delta_{\mathbf{GG'}} - v(\mathbf{q} + \mathbf{G})P_{\mathbf{GG'}}^{0}(\mathbf{q},\omega)$$
 (22)

Then according to Eqs. (11 and 13), the dielectric matrices $\epsilon_{\mathbf{GG'}}(\mathbf{q},\omega)$ have to be calculated and inverted for many values of ω . This is computationally time consuming. Nevertheless, it has been carried out by some authors^{6,15} who choose to evaluate the frequency integral by using a Gaussian integration scheme along the imaginary axis to circumvent the problem of the pole structure of the screened interaction along the real frequency axis⁶. An alternative approach is the use of a plasmon pole model^{5,10,13,36} to mimic the frequency dependence of the dielectric matrix. These models give a good description of the low frequency behavior of the dynamically screened interaction and allow the determination of an analytic expression for the frequency integral appearing in Eq. (11). We used three types of plasmon pole models to describe approximately the dependence of $\epsilon^{-1}(\omega)$ on the frequency ω . These different models were proposed by Von der Linden and Horsch¹⁰, Engel and Farid³⁶, and by Hamada *et al.*¹³ We choose to detail the first one and emphasize that the values of the quasiparticle energies are not sensitive to the model type (see Table II which details the calculated QP energies of Si with these three models).

In such an approach, we consider the symmetrized dielectric matrix $\tilde{\epsilon}_{\mathbf{G}\mathbf{G}'}(\mathbf{q},\omega)$ defined by

$$\tilde{\epsilon}_{\mathbf{GG'}}(\mathbf{q}, \omega) = \frac{|\mathbf{q} + \mathbf{G}|}{|\mathbf{q} + \mathbf{G'}|} \epsilon_{\mathbf{GG'}}(\mathbf{q}, \omega)$$
(23)

Introducing the following notation

$$M_{\mathbf{G}}^{nm}(\mathbf{k}, \mathbf{q}) = \langle \Psi_{\mathbf{k} - \mathbf{q}n} | e^{-i(\mathbf{q} + \mathbf{G}) \cdot \mathbf{r}} | \Psi_{\mathbf{k}m} \rangle$$
 (24)

and using Eqs. (23, 22, 16) leads the following result for the static symmetrized dielectric matrix

$$\tilde{\epsilon}_{\mathbf{G}\mathbf{G}'}(\mathbf{q},\omega=0) = \delta_{\mathbf{G}\mathbf{G}'} - \frac{16\pi}{\Omega|\mathbf{q} + \mathbf{G}||\mathbf{q} + \mathbf{G}'|} \sum_{v,c,\mathbf{k}} \frac{M_{\mathbf{G}}^{vc}(\mathbf{k},\mathbf{q})[M_{\mathbf{G}'}^{vc}(\mathbf{k},\mathbf{q})]^*}{\epsilon_v(\mathbf{k} - \mathbf{q}) - \epsilon_c(\mathbf{k})}$$
(25)

We then diagonalize the hermitian $\tilde{\epsilon}(\mathbf{q}, \omega = 0)$. Its real eigenvalues $\lambda_p(\mathbf{q})$ and orthonormal eigenvectors $|\phi_p(\mathbf{q})\rangle$ can be used to perform the matrix inversion according to

$$\tilde{\epsilon}^{-1}(\mathbf{q}, \omega = 0) = \sum_{p} |\phi_{p}(\mathbf{q})\rangle \frac{1}{\lambda_{p}(\mathbf{q})} \langle \phi_{p}(\mathbf{q})|$$
(26)

Von der Linden and Horsch supposed that the frequency dependency of the dielectric matrix is encompassed in the eigenvalues of the static symmetrized dielectric matrix while the eigenvectors are frequency independent

$$\tilde{\epsilon}_{\mathbf{G}\mathbf{G}'}^{-1}(\mathbf{q},\omega) = \sum_{p} \phi_{\mathbf{G}}^{p}(q) \frac{1}{\lambda_{p}(\mathbf{q},\omega)} [\phi_{\mathbf{G}'}^{p}(\mathbf{q})]^{*}$$
(27)

where

$$\frac{1}{\lambda_p(\mathbf{q},\omega)} = 1 + \frac{z_p(\mathbf{q})}{2}\omega_p(\mathbf{q})\left\{\frac{1}{\omega - (\omega_p(\mathbf{q}) - i\delta)} - \frac{1}{\omega + (\omega_p(\mathbf{q}) - i\delta)}\right\}$$
(28)

It should be noted that such a parameterization of the frequency dependence of the inverse of the eigenvalues guarantees that $\tilde{\epsilon}$ is an even function of ω . Here, two parameters have to be determined: (1) The force of the pole $z_p(\mathbf{q})$ which is defined by letting $\omega = 0$ in Eq. (28)

$$z_p(\mathbf{q}) = 1 - \lambda_p^{-1}(\mathbf{q}, 0), \tag{29}$$

and is positive since it can be shown that $\lambda_p^{-1}(\mathbf{q},0)$ lies in the interval $(0,1)^{39}$. (2) The frequency of the pole $\omega_p(\mathbf{q})$ which is determined from the Johnson's sum rule⁴⁰. If we introduce the following quantities

$$\Theta_{\mathbf{G}}^{p}(\mathbf{q}) = \frac{\phi_{\mathbf{G}}^{p}(\mathbf{q})}{|\mathbf{q} + \mathbf{G}|},\tag{30}$$

and

$$L_{\mathbf{GG'}} = (\mathbf{q} + \mathbf{G})(\mathbf{q} + \mathbf{G'})\rho(\mathbf{G} - \mathbf{G'}), \tag{31}$$

where $\rho(\mathbf{G})$ denotes a Fourier component of the charge density, we can write the frequencies of the poles according to

$$\omega_p(\mathbf{q})^2 = \frac{4\pi}{z_p(\mathbf{q})} \langle \Theta^p(\mathbf{q}) | L(\mathbf{q}) | \Theta^p(\mathbf{q}) \rangle$$
 (32)

Using the usual development of ρ and Θ along the reciprocal vectors, it can be easily shown that

$$\langle \Theta^p(\mathbf{q})|L(\mathbf{q})|\Theta^p(\mathbf{q})\rangle = \frac{1}{V} \int \rho(\mathbf{r})|\nabla \Theta(\mathbf{r})|^2 d^3\mathbf{r}$$
 (33)

where V denote the volume of the unit cell. Since $z_p(\mathbf{q})$ and the quantity defined by Eq. (33) are both positive we deduce that the frequency defined by Eq. (32) is positive. Now all the ingredients of the plasmon pole model have been defined, and we are able to give an analytic expression of the matrix elements of the self-energy in the GW approximation between LDA Bloch orbitals.

To test our implementation of the plasmon pole model, we have plotted in Fig. 1 the Engel-Farid Plasmon model band structure of Si along L, Γ , and X high symmetry directions. We have found that our implementation is in excellent agreement with the results of Engel and Farid³⁶, and Aulbur⁴¹. Indeed, for small **k** wave vectors, the lowest plasmon band shows a quadratic dispersion $\omega_0(\mathbf{k}) = \omega_0(\mathbf{0}) + \alpha |\mathbf{k}|^2$, with a dimensionless direction-dependent dispersion coefficient α (see up-triangle curve in Fig. 1). We find $\omega_0(\mathbf{0}) = 15.7$ eV and $\alpha_{\Delta} = 0.33$ in good agreement with the values of 15.91 eV and 0.34 of Engel and Farid as well as the experimental values of 16.7 eV and 0.41⁴². To check also the validity of the plasmon pole model to be used as a substitute for the dielectric function of real materials we have compared the plasmon pole model of Hamada et al.¹³ with our direct ab-initio computation of the dielectric function within the RPA including the so called local-field effects (see Fig. 2) and with available experimental results⁴² for the energy loss spectrum. We notice that the model mimics nicely our ab initio calculated dielectric function.

The matrix elements of the self-energy could be divided into an energy independent contribution Σ^{hf} and an energy dependent contribution $\Sigma(\omega)$. The first contribution corresponds to the Hartree-Fock contribution and is given by

$$\langle \Psi_{\mathbf{k}n} | \Sigma^{hf} | \Psi_{\mathbf{k}n} \rangle = -\frac{4\pi}{\Omega} \sum_{\mathbf{q}} \sum_{m \ occ} \sum_{\mathbf{G}} \frac{|M_{\mathbf{G}}^{mn}(\mathbf{k}, \mathbf{q})|^2}{|\mathbf{q} + \mathbf{G}|^2}$$
(34)

where the summation runs only over the occupied states. The energy dependent contribution can be expressed as

$$\langle \Psi_{\mathbf{k}n} | \Sigma(\omega) | \Psi_{\mathbf{k}n} \rangle = \frac{4\pi}{\Omega} \sum_{\mathbf{q},m,p} \frac{z_p(\mathbf{q})\omega_p(\mathbf{q})/2}{\omega - \epsilon_m(\mathbf{k} - \mathbf{q}) + [\omega_p(\mathbf{q}) - i\delta] sgn(\mu - \epsilon_m(\mathbf{k} - \mathbf{q}))} |\beta_p^{mn}(\mathbf{k}, \mathbf{q})|^2$$
(35)

where

$$\beta_p^{mn}(\mathbf{k}, \mathbf{q}) = \sum_{\mathbf{G}} [M_{\mathbf{G}}^{mn}(\mathbf{k}, \mathbf{q})]^* \Theta_{p\mathbf{q}}(\mathbf{G})$$
(36)

and

$$sgn(\mu - \epsilon_m(\mathbf{k} - \mathbf{q})) = \begin{cases} 1 & \text{for } \epsilon_m(\mathbf{k} - \mathbf{q}) < \mu \\ -1 & \text{for } \epsilon_m(\mathbf{k} - \mathbf{q}) > \mu \end{cases}$$

Here m denotes an electronic band index, p a plasmon band index and \mathbf{q} a vector in the Brillouin zone. It should be emphasized that the summation over m is not restricted to occupied states as in the expression of the Hartree-Fock contribution. Both the poles of the Green's function and of the screened interaction contribute to this expression.

3. Numerical details

One of the central problem within the realization of the GW approximation is the calculation of matrix elements whose type is defined by Eq. (24). Using the PAW formalism, the smooth 'pseudo wave function' $\tilde{\Psi}_{\mathbf{k}n}$ associated to an 'all-electron' LDA wave function $\Psi_{\mathbf{k}n}$ can be written

$$\tilde{\Psi}_{\mathbf{k}n} = \frac{1}{\sqrt{V}} \sum_{\mathbf{G}} A_{\mathbf{k}n}(\mathbf{G}) e^{i(\mathbf{k} + \mathbf{G}) \cdot \mathbf{r}}$$
(37)

where the sum runs over reciprocal lattice vectors. As illustrated in the part dedicated to the PAW formalism, the expectation value of $e^{-i(\mathbf{q}+\mathbf{G}).\mathbf{r}}$ can be divided into three parts according to $M_{\mathbf{G}}^{nm}(\mathbf{k},\mathbf{q}) = \langle \tilde{\Psi}_{\mathbf{k}-\mathbf{q}n}|e^{-i(\mathbf{q}+\mathbf{G}).\mathbf{r}}|\tilde{\Psi}_{\mathbf{k}m}\rangle + \langle \Psi_{\mathbf{k}-\mathbf{q}n}^{1}|e^{-i(\mathbf{q}+\mathbf{G}).\mathbf{r}}|\Psi_{\mathbf{k}m}^{1}\rangle - \langle \tilde{\Psi}_{\mathbf{k}-\mathbf{q}n}^{1}|e^{-i(\mathbf{q}+\mathbf{G}).\mathbf{r}}|\tilde{\Psi}_{\mathbf{k}m}^{1}\rangle.$ The first term, which involves plane waves is defined as

$$\sum_{\mathbf{G}'} A_{\mathbf{k}-\mathbf{q}n}^*(\mathbf{G}') A_{\mathbf{k}m}(\mathbf{G} + \mathbf{G}')$$
(38)

In our scheme, the summation over reciprocal lattice vectors in this expression takes account of a vector \mathbf{G}' if both \mathbf{G}' and $\mathbf{G} + \mathbf{G}'$ are smaller than a cutoff parameter. In general 300 \mathbf{G}' vectors were included in the summation for the systems studied here, except for Diamond

where the convergence is achieved only when 400 G' were used. The two remaining terms which involve localized contributions can be expressed as

$$\sum_{\mathbf{a}.i,j} \langle \tilde{\Psi}_{\mathbf{k}-\mathbf{q}n} | \tilde{p}_{j}^{\mathbf{a}} \rangle \left[\langle \Phi_{j}^{\mathbf{a}} | e^{-i(\mathbf{q}+\mathbf{G}).\mathbf{r}} | \Phi_{i}^{\mathbf{a}} \rangle - \langle \tilde{\Phi}_{j}^{\mathbf{a}} | e^{-i(\mathbf{q}+\mathbf{G}).\mathbf{r}} | \tilde{\Phi}_{i}^{\mathbf{a}} \rangle \right] \langle \tilde{p}_{i}^{\mathbf{a}} | \tilde{\Psi}_{m\mathbf{k}} \rangle$$
(39)

Since the overlap between the 'pseudo wave functions' and the projectors is known, we have to calculate quantities like $\langle \Phi_j^{\mathbf{a}} | e^{-i(\mathbf{q}+\mathbf{G})\cdot\mathbf{r}} | \Phi_i^{\mathbf{a}} \rangle$. Using the development of plane waves along spherical Bessel functions j_l , we get

$$\langle \Phi_j^{\mathbf{a}} | e^{-i(\mathbf{q} + \mathbf{G}) \cdot \mathbf{r}} | \Phi_i^{\mathbf{a}} \rangle = \begin{cases} 4\pi \ e^{-i(\mathbf{q} + \mathbf{G}) \cdot \mathbf{R_a}} \sum_{lm} (-i)^l \ Y_{lm}(\widehat{\mathbf{q} + \mathbf{G}}) \ G_{l_i m_i \ l_j m_j}^{lm} \\ \times \int_0^{r_c^{\mathbf{a}}} d\mathbf{r} \ r^2 \ j_l(|\mathbf{q} + \mathbf{G}||\mathbf{r}|) \ \Phi_{l_j n_j}(r) \ \Phi_{l_i n_i}(r) \end{cases}$$
(40)

where the Gaunt coefficients are defined to be

$$G_{l_i m_i \ l_j m_j}^{lm} = \sqrt{4\pi} \int d\Omega \ Y_{l_i m_i}^*(\widehat{\mathbf{r}}) \ Y_{l_m}^*(\widehat{\mathbf{r}}) \ Y_{l_j m_j}(\widehat{\mathbf{r}})$$
 (41)

The symmetrized dielectric matrix defined by Eq.(25) as well as the matrix elements of the self-energy defined by Eqs. (34) and (35) are obtained by an integration over the Brillouin zone. We used the special points' technique⁴³ in which the summation over a uniform mesh of **k**-points is reduced by symmetry to a summation over fewer special **k**-points if the integrand possesses the full symmetry of the point group of the lattice. The summation over **q**-points in the expectation value of the self-energy has to be carried out carefully, since the integrands have an integrable singularity in $\frac{1}{\mathbf{q}^2}$ for $\mathbf{q} \to 0$. This can be readily seen in the expectation value of Σ^{hf} defined by Eq. (34) where the divergence occurs when $\mathbf{G} = 0$. We follow the idea of Gygi and Baldereschi⁴⁴ introduced for fcc lattice by considering a smooth function $F(\mathbf{q})$ which reflects the translational symmetry of the Bravais lattice and which diverges as $\frac{1}{\mathbf{q}^2}$ as q vanishes. If we have to integrate a function $g(\mathbf{q})$ which behaves as $\frac{A}{\mathbf{q}^2}$ for small \mathbf{q} , we can write

$$\sum_{\mathbf{q}} g(\mathbf{q}) = \sum_{\mathbf{q}} [g(\mathbf{q}) - A F(\mathbf{q})] + A \sum_{\mathbf{q}} F(\mathbf{q})$$
(42)

Such a decomposition is illustrated for the Hartree-Fock contribution

$$\langle \Psi_{\mathbf{k}n} | \Sigma^{hf} | \Psi_{\mathbf{k}n} \rangle = -\frac{4\pi}{\Omega} \sum_{q} \sum_{m \ occ} \left[\sum_{\mathbf{G}} \frac{|M_{\mathbf{G}}^{mn}(\mathbf{k}, \mathbf{q})|^2}{|\mathbf{q} + \mathbf{G}|^2} - F(\mathbf{q}) \delta_{mn} \right] - \frac{4\pi}{\Omega} \sum_{m \ occ} \delta_{mn} \sum_{q} F(\mathbf{q})$$
(43)

The function in square brackets does not contain any divergence owing to the following property

$$\lim_{\mathbf{q} \to 0} M_{\mathbf{0}}^{mn}(\mathbf{k}, \mathbf{q}) = \delta_{mn} \tag{44}$$

and is easily integrated by special points method while the integral of $F(\mathbf{q})$ over the Brillouin zone is performed analytically. The same type of method is used to treat the $\frac{1}{\mathbf{q}^2}$ singularity in Eq. (35). Here the development of $|\beta_p^{mn}(\mathbf{k}, \mathbf{q})|^2$ shows that a divergence like $\frac{1}{q}$ also occurs. The problem can still be solved by using another function which diverges as $\frac{1}{q}$ if $\mathbf{q} \to 0$. As a matter of fact, this divergence is less severe than the previous one and does not require a special treatment since the accuracy of the numerical results is not affected if we neglect this divergence. It should be noted that the treatment of the singularity in Eq. (35) necessitates the evaluation of the symmetrized dielectric matrix for $\mathbf{q} \to 0$. As the convergence of the head element of this matrix as a function of the number of \mathbf{k} -points is slow, the calculation is performed separately. All other Brillouin zone integrations are carried out using 10 special \mathbf{k} -points, which produces accurate numerical results (see the result section).

The evaluation of the quasiparticle energies requires the determination of the renormalization factor defined by Eq. (20). The derivative of the self-energy is then evaluated by using a finite difference scheme with a step equal to 1 eV. The values of the renormalization factors are summarized in Table I for the different materials studied here. These constants Z are roughly the same for the electron and hole states. Furthermore Z is similar for all the materials considered here. The values indicate that account of dynamical renormalization is crucial to get quantitatively correct results. At the same time values of Z close to unity show that the quasiparticles are well defined and that the GW approximation is reasonable.

The last point to be discussed is the evaluation of the matrix elements of the exchangecorrelation potential which appears in Eq. (18). Here some problem arise due to the nonlinearity of the exchange-correlation potential. Indeed, in the PAW calculation, the exchange correlation potential is calculated by taking into account the valence n_v and core electron density n_c since $V_{xc}^{LDA}(\mathbf{r}) = V_{xc}^{LDA}[n_v(\mathbf{r}) + n_c(\mathbf{r})]$. Therefore, the self-energy in the GW approximation describe only the valence electrons, and we are obliged to make the assumption that the core-valence exchange and core-polarization contributions to the energy of a valence state is given by⁵

$$\langle \Psi_{\mathbf{k}n} | V_{xc\ core-val} | \Psi_{\mathbf{k}n} \rangle = \langle \Psi_{\mathbf{k}n} | V_{xc}[n_v + n_c] | \Psi_{\mathbf{k}n} \rangle - \langle \Psi_{\mathbf{k}n} | V_{xc}[n_v] | \Psi_{\mathbf{k}n} \rangle \tag{45}$$

Such a procedure is some what hidden when pseudo-potential are used since such an operation is performed in the unscreening of the pseudo-potential by subtracting $V_{xc}[n_v]$. The shortcoming of this approach is that the ionic pseudo-potential is dependent on the valence configuration, reducing the transferability of the potential. Moreover, it has been shown that including core corrections to the exchange and correlation is necessary to describe properly the structural properties of solids⁴⁵. The PAW does not suffer this shortcoming but it seems that justifying Eq. (45) is not an easy task. Considering that the argument mentioned before is correct, the quantity which must be subtracted is then defined by

$$\langle \Psi_{\mathbf{k}n} | V_{xc}^{LDA}[n_v(\mathbf{r})] | \Psi_{\mathbf{k}n} \rangle = \begin{cases} \langle \tilde{\Psi}_{\mathbf{k}n} | V_{xc}^{LDA}[\tilde{n}_v(\mathbf{r})] | \tilde{\Psi}_{\mathbf{k}n} \rangle + \sum_{i,j,a} \langle \tilde{\Psi}_{n\mathbf{k}} | \tilde{p}_i^a \rangle \\ \times \left[\langle \Phi_i^a | V_{xc}^{LDA}[n_v^1(\mathbf{r})] | \Phi_j^a \rangle - \langle \tilde{\Phi}_i^a | V_{xc}^{LDA}[\tilde{n}_v^1(\mathbf{r})] | \tilde{\Phi}_j^a \rangle \right] \langle \tilde{p}_j^a | \tilde{\Psi}_{n\mathbf{k}} \rangle \end{cases}$$

$$(46)$$

Table III shows the matrix elements of the exchange-correlation potential of Si calculated using the PAW formalism compared to the results obtained by means of the LAPW method¹³. The agreement between our results and the results of Hamada $et\ al.$ is remarkably good if we consider that these results are based on different calculation schemes and that different parameterizations of the exchange-correlation energy are used.

4. Use of symmetry to reduce computational cost

If $\Psi_{\mathbf{k}n}$ is a Bloch wave function solution of the Kohn-Sham equation and R a symmetry operation belonging to the point group of the crystal which we suppose to be symmorphic,

we can write the way the Bloch wave function transform under such a symmetry operation

$$\Psi_{\mathbf{k}n}(R^{-1}\mathbf{r}) = \sum_{m} D(R)_{nm} \Psi_{\mathbf{k}m}(\mathbf{r}), \tag{47}$$

where $D(R)_{nm}$ denote the unitary transformation associated to the symmetry operation R. If the state $\Psi_{\mathbf{k}n}$ is non degenerated, the transformation rule of the wave function simplify greatly since $D(R)_{nm} = \delta_{nm}$. We suppose now that the states considered here are non degenerated to simplify the discussion. Using such a relation it can be shown that the matrix elements defined by Eq. (24) satisfy the following relation

$$M_{\mathbf{G}}^{nm}(\mathbf{k}, R\mathbf{q}) = M_{R^{-1}\mathbf{G}}^{nm}(\mathbf{k}, \mathbf{q}) \quad \text{for } R\mathbf{k} = \mathbf{k},$$
 (48)

that means for the symmetry operations belonging to the little group $G_{\mathbf{k}}$ of the point group G. Then, it can be proved that the integrand appearing in the Hartree-Fock contribution defined by Eq. (34) is invariant under symmetry operations belonging to $G_{\mathbf{k}}$. Such a symmetry property reduces the number of \mathbf{q} -points for which the integrand has to be calculated. Indeed, if $BZ_{\mathbf{k}}$ denotes the irreducible Brillouin zone defined by $G_{\mathbf{k}}$, the Hartree-Fock contribution can be rewritten as

$$\langle \Psi_{\mathbf{k}n} | \Sigma^{hf} | \Psi_{\mathbf{k}n} \rangle = -\frac{4\pi}{\Omega} \sum_{\mathbf{q} \in BZ_{\mathbf{k}}} w(\mathbf{q}) \sum_{m \ occ} \sum_{\mathbf{G}} \frac{|M_{\mathbf{G}}^{mn}(\mathbf{k}, \mathbf{q})|^2}{|\mathbf{q} + \mathbf{G}|^2}$$
(49)

where $w(\mathbf{q})$ denotes the weight of the \mathbf{q} -point. It should be noted here that the term we have subtracted from this expression to cancel the Coulomb singularity does not give rise to complications since this term is invariant under all symmetry operations of G. Moreover, if the state $\Psi_{\mathbf{k}n}$ is degenerated, we should sum the matrix elements over all degenerated states to get a true invariant integrand. The same type of symmetry reduction holds for the calculation of the symmetrized static dielectric matrix using the fact that

$$M_{\mathbf{G}}^{nm}(R\mathbf{k}, \mathbf{q}) = M_{R^{-1}\mathbf{G}}^{nm}(\mathbf{k}, \mathbf{q}) \quad \text{for } R\mathbf{q} = \mathbf{q}$$
 (50)

and

$$\epsilon_n(R\mathbf{k}) = \epsilon_n(\mathbf{k}) \tag{51}$$

We then get

$$\tilde{\epsilon}_{\mathbf{G}\mathbf{G}'}(\mathbf{q},\omega=0) = \delta_{\mathbf{G}\mathbf{G}'} - \frac{16\pi}{\Omega|\mathbf{q} + \mathbf{G}'|} \sum_{\mathbf{k} \in BZ_{\mathbf{q}}} \sum_{v,c} \sum_{R \in G_{\mathbf{q}}} \frac{M_{RG}^{vc}(\mathbf{k}, \mathbf{q})[M_{RG'}^{vc}(\mathbf{k}, \mathbf{q})]^{*}}{\epsilon_{v}(\mathbf{k} - \mathbf{q}) - \epsilon_{c}(\mathbf{k})}$$
(52)

The relationship between the matrix elements of $\tilde{\epsilon}_{\mathbf{G}\mathbf{G}'}$ also reduces the computational cost. Using the symmetry property of the symmetrized dielectric function $\tilde{\epsilon}(\mathbf{r}, \mathbf{r}') = \tilde{\epsilon}(R\mathbf{r}, R\mathbf{r}')$, it can be shown that

$$\tilde{\epsilon}_{\mathbf{G}\mathbf{G}'}(R\mathbf{q},\omega=0) = \tilde{\epsilon}_{R^{-1}\mathbf{G}R^{-1}\mathbf{G}'}(\mathbf{q},\omega=0).$$
 (53)

So both the hermiticity of $\tilde{\epsilon}$ and the relationship between the matrix elements which results from the symmetry operations leaving \mathbf{q} invariant are used to reduce the number of matrix elements to be computed. Now, we have to remember that the plasmon pole parameters are obtained by solving an eigenvalue problem

$$\int d\mathbf{r}' \ \tilde{\epsilon}(\mathbf{r}, \mathbf{r}') \ \phi^p(\mathbf{q}, \mathbf{r}') = \lambda_p(\mathbf{q}) \ \phi^p(\mathbf{q}, \mathbf{r})$$
(54)

By analogy with the resolution of the Schrödinger type equation in a crystal, it can be shown that

$$\phi_{\mathbf{G}}^{p}(R\mathbf{q}) = \phi_{R^{-1}\mathbf{G}}^{p}(\mathbf{q}) \quad \text{and} \quad \lambda_{p}(R\mathbf{q}) = \lambda_{p}(\mathbf{q})$$
 (55)

These symmetry properties with Eqs. (29, 30, and 32) can be used to show that

$$z_p(R\mathbf{q}) = z_p(\mathbf{q})$$
 and $\omega_p(R\mathbf{q}) = \omega_p(\mathbf{q})$ (56)

If the point group G of the crystal does not contain the inversion symmetry, the time reversal symmetry could also be implemented. Because of these symmetry relations, the eigenvectors and eigenvalues of the symmetrized dielectric matrix are only computed for irreducible \mathbf{q} -points with respect to the point group of the crystal. Now it can be demonstrated that the integrand appearing in the dependent energy contribution to the matrix element of the self-energy defined by Eq. (35) is invariant under symmetry operations belonging to the little group of \mathbf{k} denoted $G_{\mathbf{k}}$ as in the case of the Hartree-Fock contribution.

5. Parallelization

Because GWA is computationally involved the calculation of QP properties in a sequential computer is time consuming. We have used the message passing interface (MPI) to parallelize our numerical code on an IBM SP2. The most straitforward parallelization which we were able to perform was any loop or a summation involving **k**-point mesh over the Brillouin zone. First, the irreducible **k**-point with respect to the point group of the crystal were distributed on different processors. Then each processor diagonalize the Hamiltonian for a certain number of **k**-points. It then evaluates the symmetrized dielectric function and calculates the ingredients of the plasmon-pole model. Second, each processor calculates the self-energy correction for a certain number of **k**-points. and the results are gathered by the root processor to get the GW correction. This simple parallelization scheme made our computer code run much fast on the IBM SP2. Our choice of the the **k**-point mesh was also motivated by a future parallelization of the LDA eigenvalue problem for systems with many atoms per unit cell. We can set different pools of processors, and each pool will produce the diagonalization of a large Hamiltonian in parallel making the code highly scalable with the number of atoms of the system.

III. GW QUASIPARTICLE RESULTS

A. Quasiparticle results for small and medium band-gap semiconductors: Si, GaAs, AlAs, InP, and Mg₂Si

In this subsection we present the electronic structure of several small and medium gap semiconductors which are used as tests for the implementation of our all-electron PAW-GWA method. As mentioned earlier, we have implemented three different types of plasmon-pole models available in the literature, ^{10,13,36} and compared the resulting quasiparticle energies of Si for high symmetry points. Table II shows that these quasiparticle energies are not sensitive to the type of plasmon-pole model used to mimic the frequency dependence of the

screened interaction. This trend has been confirmed for the other semiconductors studied in this paper and was already mentioned in the seminal work of Hedin⁴ on the Jellium model. Then we made a detailed comparison with the only full-potential GW calculation of Hamada et al. 13 where LAPW-GWA calculation of the band structure of Si is presented. Table III compares different key ingredients necessary to evaluate the quasiparticle energies of Si in the GW approximation. Our calculated matrix elements of the exchange-correlation potential $\langle \Psi_{\mathbf{k}n}|V_{xc}^{LDA}[n_v(\mathbf{r})]|\Psi_{\mathbf{k}n}\rangle$ are compared to those obtained by LAPW-GWA. The agreement with LAPW is excellent and reflects the accuracy our LDA results obtained by PAW method. We have also compared the screened exchange (SEX) and Coulomb-hole (COH) contributions to the self-energy with the results of Hamada $et\ al.^{13}$ and of Hybertsen and Louie⁵. To make this comparison reliable, we have used the same type of plasmon-pole model than Hamada et al. We have found that the agreement of ours results with these of Hamada et al. is not fully satisfactorily, but our results are very close to the results of Hybertsen-Louie although their calculation is a pseudopotential one and uses another type of plasmon-pole model. This observation makes us confident with the PAW-GWA results and confirms the fact, as outlined before, that the detailed structure of the screened interaction is not important to determine the quasiparticle energies. We should point out here that $\Sigma = \Sigma_{SEX} + \Sigma_{COH}$ which enters the calculation of the quasiparticle energies are close to each other whether we consider the PAW, the LAPW, or the Pseudo-Potential implementations.

To calculate the quasiparticle energies it is important to correctly determine the quasiparticle renormalization factor $Z_{n\mathbf{k}}$ (see Eq. I). As stated earlier, Table I presents $Z_{n\mathbf{k}}$ calculated for the top valence state at the Γ point and for the lowest conduction state of all semiconductors studied in this paper. These values are in good agreement with the results of Hybertsen and Louie⁵ and they seem to be material and state independent and are at the vicinity of 0.8.

Tables IV, V, VI, VII, and VIII represent the calculated PAW-LDA and PAW-GWA band energies for the high symmetry points Γ , X, and L for small and medium band gap

semiconductors: Si, GaAs, AlAs, InP, and Mg₂Si, respectively (The energy scale is relative to the top of the valence state maximum). These results are compared to other GWA calculations obtained using LAPW (for Si) or PP for the other systems as well as to available experimental data⁵²⁻⁶³. In these tables we have presented our results for 2 Chadi-Cohen k-points⁴⁶ which correspond to 32 k-points in the whole Brillouin zone (BZ) (results shown between parentheses) as well as the most converged values using 10 special k-points⁴³ corresponding to 256 k-points in the BZ. We notice that most of the data in the literature are produced with about 32 k-points in the BZ, and are in excellent agreement with our unconverged values, however only the converged values should be compared to experiment. In our case we have found that the QP eigenvalues are converged with a k-point mesh beyond 256 points. The discrepancy between our GW values and others is often traced to differences between LDA values. It's also worth mentioning that Shirley et al.'s GW results for GaAs¹⁷ agree well with our results (see Table V) despite that they are of PP type, and that their calculation shows that only the inclusion of core-polarization effect produce gaps in agreement with experiment.

Fig. 3 presents the corresponding band structure along the $L\Gamma$ and ΓX high symmetry directions calculated within the LDA and GWA. We notice an overall improvement of the excited states eigenvalues compared to these obtained in LDA, whereas the LDA valence states eigenvalues are already in good agreement with experiment and GWA results do not change this agreement. In all these small and medium band gap semiconductors we remark also an average energy shift of the conduction states towards the high energies compared to LDA. This energy shift is about the same for Si and GaAs and is about 0.6 eV, and increases to about 0.8 eV for AlAs and InP. To be more specific we studied the range of applicability of the so called scissors-operator shift. To this end we have evaluated the deviation of the difference of LDA and GWA direct band gap determined at the Γ , X, and L symmetry points. We have found that these deviation of the GWA and LDA energy differences are the lowest for Si, and Mg₂Si. The maximum deviation is about 0.06, and 0.04 eV, respectively, and it occurs from L to Γ in both materials. The deviations are somewhat

larger for GaAs, AlAs, and InP, and the maximum deviation is about, 0.16, 0.15, and 0.13 eV, respectively. They are all from Γ to X. These small deviations indicate that the GWA does not change much the LDA dispersion across the Brillouin zone, justifying the use of the scissors-operator shift for the calculation of the dielectric function for small and medium band gap semiconductors^{47–49}. We will see in the next subsection that such deviations are much larger in absolute values for wide-band-gap semiconductors.

As for Mg₂Si we believe that it is the first time that this compound is studied within the GW approximation. The PAW-LDA and PAW-GWA band energies for the high symmetry points Γ , X, and L are shown in table VIII. Due to the lack of photoemission experiments, the GW results are compared with optical measurements, making the assumption that excitonic effects are negligible. The GWA results are in good agreement with the experimental results and compare favorably with the EPM calculation of Au-Yang et al.⁵⁰ Fig. 3 presents the corresponding band structure along the $L\Gamma$ and ΓX high symmetry directions within the LDA and GWA.

Fig. 4 shows the LDA and GWA calculated minimum band gaps for all studied semiconductors, and are compared to the experimental results. A perfect agreement with experiment is achieved when the calculated value falls on the dashed line. We notice that for most of the small and medium gap semiconductors GWA does not account for the whole correction of the band gap. The disagreement with experimental band gaps is most probably due to the procedure used to decouple the core and valence electrons. Indeed, we used the LDA exchange-correlation potential with the valence electron density to estimate the LDA counterpart of the self-energy and we believe that a more refined treatment should rely on the evaluation of the core-valence exchange interaction within the Hartree-Fock approximation.⁴ However, this latter suggested procedure is difficult to implement in our formalism and the outcome would not necessarily improve upon the former simple scheme. On the other hand, it is interesting to mention that a first order vertex and self-consistent corrections to the RPA polarizability and to the self-energy within the GWA increase the direct energy band gaps of Si at the Γ , L, and X points by about 0.36, 0.44, and 0.39 eV, respectively¹¹. It

seems then that there is no compensation between the vertex correction and the selfconsistency as original thought. If we start from our converged Si GWA results, and use these latter results we could improve the agreement between our calculated band gaps and experimentent. However, when some PP-GWA results are used, the additional corrections overestimates the experimental gaps. At the present time it looks like the question of the band gaps is not fully solved. It is also important to remark that these vertex corrections and the corrections arising from the selfconsistency are not quite accurate since the starting point of these calculations is a noninteracting Green's function instead of the selfconsistent Green's function as suggested by Hedin³.

B. Quasiparticle results for wide band gap semiconductors and insulators: C, and LiCl

It is of interest to compare all-electron GWA calculations for wide band gap semiconductors and insulators to existing PP calculations. Wide band gap semiconductors are somehow puzzling in contrast to small and medium semiconductors: While the LDA band gap of these materials are significantly underestimated compared to experiment, the LDA static dielectric function are usually in good agreement with experimental results, see for instant Ref.^{47,49}.

Tables IX, and X show the calculated PAW-LDA and PAW-GWA band energies for the high symmetry points Γ , X, and L for wide band gap semiconductors: C, and LiCl, respectively (The energy scale is relative to the top of the valence state maximum). These results are compared to other GWA calculations obtained using PP-GWA method^{5,51} and to experimental data whenever available^{52,64-66}. Fig. 5 presents the corresponding band structure along the $L\Gamma$ and ΓX high symmetry directions within the LDA and GWA. The C and LiCl values have been computed using 32 k-points as well as 256 k-points in the Brillouin zone. The results of the two sets of k-points are in good agreement showing that the set of 32 k-points is good enough. For C the calculated QP eigenvalues are in good agreement with experiment and the PP calculations. For LiCl only the experimental band

gap is available and is slightly larger than our GW value. It's worth mentioning that we didn't update the Green function to get our GW values. Such a procedure leads to an increase of the GW band gap by about 0.3 eV and then to a better agreement between our results and PP results of Hybertsen and Louie⁵. For these wide-gap materials we looked also to the applicability of the scissors-operator shift. We calculated the maximum change of the difference between the GWA and LDA direct band gap at the Γ , X, and L symmetry points. We found that the maximum deviation across the Brillouin zone is for C and is about 0.32 eV. It occurs for the L and Γ differences, whereas it is about 0.28 eV for LiCl and occurs for X and Γ energy differences. These deviations seem to be somewhat larger in absolute values (about twice the value found for GaAs) than for small and medium-gap semiconductors, and may make the use of the scissors-operator shift, for the computation of the optical properties, less applicable. However, if we compare these energy deviations to the size of the band gap, we find that the largest ratio occurs for C and is only 5%, whereas it is about 10% for a medium gap semiconductor such as GaAs.

IV. CONCLUSION

We have implemented a GWA based on an all-electron method using the recently developed projector augmented wave (PAW) method.³⁵ The knowledge of the one-electron Green function of the PAW Hamiltonian allows us to construct the quasiparticle self-energy within the GWA, in which the dynamical screening of the electron-electron interaction arises from a plasmon model dielectric function^{10,13,36} for which the parameters are adjusted to the dielectric function calculated using the random-phase-approximation (RPA). We have tried various plasmon model dielectric functions for the screening of the Coulomb interaction and showed that the quasiparticle energies are insensitive to the type of the model used.

Using this new GWA method, we have determined for the first time the GWA quasiparticle electronic structure of Mg₂Si. We have found that our LDA results are in good agreement with the empirical pseudopotential, and that the GWA shifts almost rigidly the empty states by about 0.32 eV towards higher energies.

Concerning the other semiconductors studied here, we have found an overall agreement of our calculated electronic structure of various semiconductors with existing GWA pseudopotential calculations performed by different groups^{5,8,14,17,51}, and with experimental results^{52,64-66,53-58,60-63,59}. However, for detailed comparisons, the all-electron GWA band gaps are slightly smaller that most of the PP results. Nevertheless, some of the PP results¹⁷ are much closer to ours. One of the possible source of the all-electron results compared to the PP ones is the way the decoupling of the core and valence electrons is done. In the PP approach this decoupling is some what hidden. In fact, we have used the LDA exchangecorrelation potential with the valence electron density to remove the LDA counterpart of the self-energy. We believe that a more refined treatment should rely on the evaluation of the core-valence exchange interaction within the Hartree-Fock approximation⁴ which we find difficult to implement in our current all-electon PAW-GWA approach. On the other hand, the first order vertex and self-consistent corrections to the RPA polarizability and to the self-energy within the GWA are shown to increase the direct energy band gaps of Si at the Γ , L, and X points by few tenths of an eV¹¹. It seems then that there is no compensation between the vertex correction and the selfconsistency as it was always assumed. However, these corrections are not quite accurate since the starting point of these calculations is a noninteracting Green's function instead of the selfconsistent Green's function as suggested by $Hedin^3$.

To our knowledge this is the first all-electron GWA calculation that has corrected LDA eigenvalues for three type of semiconductors: small, medium, and wide band gap, and that questioned the correctness of the band gap of semiconductors obtained by means of PP-GWA. We hope that this work would be used as a reference and triggers off further interest on an all-electron GW approach.

V. ACKNOWLEDGMENT

We would like to thank P. Blöchl for providing us with his PAW code and for useful discussions. Part of this work was done during our visit to the Ohio State University, and we would like to thank J. W. Wilkins and W. Aulbur for useful discussions. The Supercomputer time was granted by CINES on the IBM SP2 supercomputer (project gem1100).

REFERENCES

- ¹ P. Hohenberg and W. Kohn, Phys. Rev. **136** (1964); W. Kohn and L.J Sham, Phys. Rev. **140**, A1113 (1965).
- ² L. Hedin and B. I. Lundqvist, J. Phys. C 4, 2064 (1971); U. von Barth and L. Hedin, J. Phys. C 5,1629 (1972).
- ³ L. Hedin, Phys. Rev. **139**, A796 (1965).
- ⁴ L. Hedin and S. Lundquist, in *Solid State Physics*, edited by H. Ehrenreich, F. Seitz, and D. Turnbull (Academic, New York, 1969), Vol. 23, p. 1.
- ⁵ M. S. Hybertsen and S. G. Louie, Phys. Rev. B **34**, 5390 (1986); Comments Cond. Mat. Phys. **13**, 223 (1987).
- ⁶ R. W. Godby, M. Schlüter, and L.J. Sham, Phys. Rev. B **37**, 10159 (1988).
- 7 R. W. Godby, and M. Schlüter, Phys. Rev. B 35, 4170 (1987).
- ⁸ R. W. Godby, and R.J. Needs, Phys. Rev. Lett. **62**, 1169 (1989).
- ⁹ W. von der Linden, P. Fulde, and K.-P. Bohnen, Phys. Rev. B **34**, 1063 (1986).
- $^{10}\,\mathrm{W}.$ von der Linden and P. Horsch, Phys. Rev. B $\boldsymbol{37},\,8351,\,8351$ (1988).
- ¹¹ R. T. Ummels, P. A. Bobbert and W. van Haeringen, Phys. Rev. B **57**, 11962 (1998).
- ¹² P. A. Bobbert and W. van Haeringen, Phys. Rev. B **49**, 10326 (1994).
- 13 N. Hamada, M. Hwang and A.J. Freeman, Phys. Rev. B $\bf 41,\,3620$ (1990).
- $^{14}\,\mathrm{R.}$ Hott, Phys. Rev. B 44, 1057 (1991).
- $^{15}\,{\rm F.}$ Aryasetiawan, Phys. Rev. B ${\bf 46},\,13051$ (1992).
- ¹⁶ E. L. Shirley and S. G. Louie, Phys. Rev. Lett. **71**, 331993.
- $^{17}\,\mathrm{E.}$ L. Shirley, X. Zhu, and S. G. Louie, Phys. Rev. Lett. $\mathbf{69},\,2955$ (1992).

- ¹⁸ F. Araysetianwan and O. Gunnarsson, Rep. Prog. Phys. **61**, 237-312 (1998).
- ¹⁹ W. G. Aulbur, L. Jönsson, and J. W. Wilkins, 'Quasiparticle calculations in solids', to be published in Solid state Physics; edited by H. Ehrenreich.
- ²⁰ N. I. Kulikov, M. Alouani, M. A. Khan, and M. V. Magnitskaya, Phys. Rev. B 36, 929 (1987).
- ²¹ M. M. Steiner, R. C. Albers, and L. J. Sham, Phys. Rev. B **45**, 13272 (1992).
- ²² J. P. Perdew and M. Levy, Phys. Rev. Lett. **51**, 1884 (1983).
- ²³ L. J. Sham and M. Schlueter, Phys. Rev. Lett. **51**, 1888 (1983).
- ²⁴ J. E. Northrup, M. S. Hybertsen, and S. G. Louie, Phys. Rev. B **39**, 8198 (1989).
- ²⁵ S. Saito, S. B. Zhang, S. G. Louie, and M. L. Cohen, Phys. Rev. B **40**, 3643 (1989).
- ²⁶ X. Zhu and S. G. Louie, Phys. Rev. B **43**, 12146 (1991).
- ²⁷ J. E. Northrup, Phys. Rev. B **47**, 10032 (1993).
- ²⁸ S. B. Zhang, M. L. Cohen, S. G. Louie, D. Tománek, and M. S. Hybertsen, Phys. Rev. B 41, 10058 (1990).
- ²⁹ S. B. Zhang, M. S. Hybertsen, M. L. Cohen, S. G. Louie, and D. Tománek, Phys. Rev. Lett. 63, 1495 (1989).
- $^{30}\,\mathrm{E.}$ L. Shirley and R. M. Martin, Phys. Rev. B $\mathbf{47},\,15404$ (1993)
- ³¹ J. P. A. Charlesworth, R. W. Godby, R. J. Needs, L. J. Sham, Mat.Science and Eng. B-Solid State Mat. Adv. Tech. 14, 262 (1992).
- 32 S. Albrecht, L. Reining, R. Del Sole, and G. Onida, Phys. Rev. Lett. 80, 4510 (1998).
- ³³ L. X. Benedict, E. L. Shirley, and R. B. Bohn, Phys. Rev. Lett. **80**, 4514 (1998); Phys. Rev. B **57**, R9385 (1998).

- ³⁴ M. Rohlfing and S. G. Louie, Phys. Rev. Lett. **81**, 2312 (1998).
- ³⁵ P.E Blöchl, Phys. Rev. B **50**, 17953 (1994).
- ³⁶ G. E. Engel and B. Farid, Phys. Rev. B **47**, 15931 (1993).
- ³⁷ S.L. Adler, Phys. Rev. **126**, 413 (1962); N. Wiser, Phys. Rev. **129**, 62 (1963).
- ³⁸ L. Hedin, Int. J. of Quantum Chem. **56** 445-459 (1995).
- 39 R. Car, E. Tosatti, S. Baroni and S. Leelaprute, Phys. Rev. B $\mathbf{24},\,985$ (1981).
- ⁴⁰ D. L. Johnson, Phys. Rev. B **9**, 4475 (1974).
- ⁴¹ W. G. Aulbur, PhD thesis, The Ohio State University, 1996.
- ⁴² H. Raether, Excitation of plasmons and Interband Tansitions by Electrons. Springer Tracts in Modern Physics Vol. 88 (Springer, New York, 1980).
- ⁴³ H. J. Monkhorst and J.D. Pack, Phys. Rev. B **13**, 5188 (1976).
- $^{44}\,\mathrm{F.}$ Gygi and A. Baldereschi, Phys. Rev. B $\mathbf{34},\,4405$ (1986).
- ⁴⁵ S. G. Louie, S. Froyen and M. L. Cohen, Phys. Rev. B **26**, 1738 (1982).
- ⁴⁶ J. Chadi and M. L. Cohen, Phys. Rev. B **8**, 5747 (1973).
- ⁴⁷ J. Chen, Z. H. Levine, and J. W. Wilkins, Appl. Phys. Lett. **66**, 1129 (1995).
- ⁴⁸ Z. H. Levine and D. C. Allan, Phys. Rev. B **43**, 4187 (1991).
- ⁴⁹ M. Alouani and J. M. Wills, *Excited states calculated by means of the linear muffin-tin orbital method*, Springer series (to be published); and Phys. Rev. B **54**, 2480 (1996).
- ⁵⁰ M. Y. Yang and M. L. Cohen, Phys. Rev. **178**, 1358 (1969); and Solid Stat. Comm. **6**, 855 (1968).
- $^{51}\,\mathrm{M}.$ Rohlfing, Peter Krüger and J. Pollmann, Phys. Rev. B $\mathbf{48},\,17791$ (1993).

- ⁵² Numerical Data and Functional Relationships in Science and Technology, edited by K.H. Hellwege and O. Madelung, Landolt-Börnstein, New Series, Group III, Vols. 17a and 22a (Springer, Berlin, 1982).
- ⁵³ J.E. Ortega and F.J. Himpsel, Phys. Rev. B **47**, 2130 (1993).
- ⁵⁴ W.E. Spicer and R. C. Eden, in *Proceedings of the Ninth International Conference on the Physics of Semiconductors*, Moscow, 1968, edited by S. M. Ryvkin (Nauka, Leningrad, 1968), Vol. 1, p. 61.
- ⁵⁵ A. L. Wachs, T. Miller, T. C. Hsieh, A.P. Shapiro, and T.C. Chiang, Phys. Rev. B 32, 2326 (1985).
- ⁵⁶ F.J. Himpsel, P. Heimann, and D.E. Eastman, Phys. Rev. B **24**, 2003 (1981).
- 57 R. Hulthen and N. G. Nilsson, Solid State Commun. 18, 1341 (1976).
- ⁵⁸ D. Straub, L. Ley, and F.J. Himpsel, Phys. Rev. Lett. **54**, 142 (1985).
- 59 D. J. Wolford and J.A. Bradley, Solid State Commun. $\mathbf{53}$, 1069 (1985).
- ⁶⁰ D.E. Aspnes and A. A. Studna, Phys. Rev. B **27**, 985 (1983); D. E. Aspnes, S. M. Kelso, R.A. Logan, and R. Bhatt, J. Appl. Phys. **60**, 754 (1986).
- ⁶¹ M. Cardona, N.E. Christensen, and G. Fasol, Phys. Rev. B **38**, 1806 (1988).
- ⁶² P. Lautenschlager, M. Garriga, S. Logothetidis, and M. Cardonna **35**, 9174 (1987).
- ⁶³ M. W. Heller and G. C. Damielson, J. Phys. Chem. Solids **23**, 601 (1962).
- $^{64}\,\mathrm{F.R.}$ McFeely et al., Phys. Rev. B **9**, 5268 (1974).
- 65 F.J. Himpsel, J. F. van der Veen, and D.E. Eastman, Phys. Rev. B $\mathbf{22}$, 1967 (1980).
- ⁶⁶ G. Baldini and B. Bosacchi, Phys. Status Solidi 38, 325 (1970).

TABLES

TABLE I. The renormalization constants Z for the hole state at the top of the valence band (VBM) and the electron state near the bottom of the conduction band (CBM) for C, Si, GaAs, AlAs, InP and SiMg₂.

	С	Si	GaAs	AlAs	InP	${ m Mg_2Si}$
$\mathrm{Z}_{\mathrm{V}_{BM}}$	0.85	0.80	0.80	0.81	0.79	0.76
$\mathbf{Z}_{\mathbf{C}_{BM}}$	0.87	0.81	0.81	0.82	0.82	0.79

TABLE II. Quasiparticle (QP) energies of Si for several states (in eV) and for three different types of plasmon-pole models. We notice that the QP energies are less sensitive to the type of plasmon pole model used.

	Plasmon-pole model						
	Von der Linden and Horsch a	Hamada $et \ al^b$	Engel-Farid c				
$\overline{oldsymbol{\Gamma}_{1v}}$	-12.01	-11.99	-11.89				
$oldsymbol{\Gamma}_{25'v}$	0.00	0.00	0.00				
$oldsymbol{\Gamma}_{15c}$	3.09	3.07	3.12				
$\Gamma_{2'c}$	3.88	3.86	3.86				
\mathbf{X}_{1v}	-7.97	-7.96	-8.01				
\mathbf{X}_{4v}	-3.00	-3.00	-3.01				
\mathbf{X}_{1c}	1.01	0.99	1.04				
$\mathbf{L}_{2'v}$	-9.73	-9.72	-9.75				
\mathbf{L}_{1v}	-7.21	-7.20	-7.19				
$\mathbf{L}_{3'v}$	-1.25	-1.25	-1.29				
\mathbf{L}_{1c}	1.96	1.94	1.94				
\mathbf{L}_{1c}	3.85	3.83	3.86				

aRef. 10, bRef. 13, cRef. 36

TABLE III. Matrix elements of the exchange-correlation potential and of the screened exchange (SEX) and the Coulomb hole (COH) contributions to the self-energy of Si for several states (in eV). The V_{XC} is in excellent agreement with the LAPW results¹³, whereas the SEX and COH are much closer to the PP work of Hybertsen and Louie⁵ and disagree with the LAPW results.

	V_{XC}		Σ_{SEX}			Σ_{COH}		
	Present	LAPW^a	Present	LAPW	$\mathrm{H}\text{-}\mathrm{L}^b$	Present	LAPW	H-L
$\overline{oldsymbol{\Gamma}_{1v}}$	-10.59	-10.60	-3.81	-4.44		-7.46	-6.97	
$\Gamma_{25'v}$	-11.44	-11.41	-3.44	-4.01	-3.56	-8.66	-7.80	-8.41
$oldsymbol{\Gamma}_{15c}$	-10.17	-10.19	-1.80	-1.95		-8.32	-7.68	
$oldsymbol{\Gamma}_{2'c}$	-11.29	-11.25	-1.59	-1.90		-9.30	-8.43	
\mathbf{X}_{1v}	-10.97	-10.98	-3.92	-4.56		-7.90	-7.23	
\mathbf{X}_{4v}	-10.74	-10.73	-3.49	-3.89		-8.10	-7.48	
\mathbf{X}_{1c}	-9.15	-9.17	-1.76	-1.85	-1.65	-7.50	-7.09	-7.40
$\mathbf{L}_{2'v}$	-10.97	-10.97	-3.97	-4.70		-7.78	-7.11	
\mathbf{L}_{1v}	-10.35	-10.37	-3.65	-3.92		-7.64	-7.29	
$\mathbf{L}_{3'v}$	-11.20	-11.18	-3.47	-4.02		-8.46	-7.65	
\mathbf{L}_{1c}	-10.28	-10.30	-1.87	-2.08		-8.34	-7.68	
\mathbf{L}_{1c}	-9.77	-9.77	-1.64	-1.81		-8.08	-7.43	

 $[\]overline{{}^a\mathrm{Ref.}^{13}, {}^b\mathrm{Ref.}^5}$

TABLE IV. Quasiparticle energies of Si for several states (in eV). The calculation of the self-energy is performed using 10 special **k**-points, 200 bands and 283 reciprocal lattice vectors. The size of the polarizability matrix is 137×137 and the plasmon pole model of von der Linden and Horsch¹⁰ is used. Here E_g is the minimum band gap.

	LDA		GW approximation			$\mathrm{Expt.}^a$	
	Present	LAPW^b	Present	LAPW^b	$(\mathrm{HL})^c$		
$\overline{\Gamma_{1v}}$	-12.05	-11.95	-12.01 (-11.99)	-12.21	-12.04	-12.5±0.6	
Γ_{25v}'	0.00	0.00	0.00 (0.00)	0.00	0.00	0.00	
$oldsymbol{\Gamma}_{15c}$	2.51	2.55	3.09(3.23)	3.30	3.35	$3.40, 3.05^d$	
Γ_{2c}'	3.10	3.17	3.88 (4.02)	4.19	4.08	$4.23, 4.1^d$	
\mathbf{X}_{1v}	-7.88	-7.82	-7.97 (-8.07)	-8.11			
\mathbf{X}_{4v}	-2.87	-2.84	-3.00 (-3.04)	-3.03	-2.99	-2.9^e , -3.3 ± 0.2^f	
\mathbf{X}_{1c}	0.56	0.65	1.01 (1.12)	1.14	1.44	1.25^{d}	
\mathbf{X}_{4c}	10.01		10.69 (10.77)				
\mathbf{L}_{2v}'	-9.70	-9.63	-9.73 (-9.81)	-9.92	-9.79	-9.3 ± 0.4	
\mathbf{L}_{1v}	-7.04	-6.98	-7.21 (-7.26)	-7.31	-7.18	-6.7 ± 0.2	
\mathbf{L}_{3v}'	-1.20	-1.19	-1.25 (-1.29)	-1.26	-1.27	$-1.2\pm0.2, -1.5^g$	
\mathbf{L}_{1c}	1.37	1.43	1.96 (2.06)	2.15	2.27	$2.1^h, 2.4 \pm 0.15$	
\mathbf{L}_{3c}	3.27	3.35	3.85 (3.96)	4.08	4.24	4.15 ± 0.1^{g}	
E_g gap	0.43	0.52	0.88 (1.03)	1.01	1.29	1.17	

 $[\]overline{{}^{a}\mathrm{Ref.}^{52}, \, {}^{b}\mathrm{Ref.}^{13}, \, {}^{c}\mathrm{Ref.}^{5}, \, {}^{d}\mathrm{Ref.}^{53}, \, {}^{e}\mathrm{Ref.}^{54}, \, {}^{f}\mathrm{Ref.}^{55}, \, {}^{g}\mathrm{Ref.}^{56}, \, {}^{h}\mathrm{Ref.}^{57}, \, {}^{i}\mathrm{Ref.}^{58}.}$

TABLE V. Quasiparticle energies of GaAs for several states (in eV). The calculation of the self-energy is performed using 10 special **k**-points, 200 bands and 307 reciprocal lattice vectors. The size of the polarizability matrix is 169×169 and the plasmon pole model of von der Linden and Horsch¹⁰ is used. Our results are compared with those of Rohlfing et al⁵¹ and those of Shirley et al¹⁷. The results of Shirley are given without (with) core polarization effects. Here E_g is the minimum band gap.

	LDA		GW	GW approximation			
	Present	$(RKP)^b$	Present	$(RKP)^b$	$(SZL)^c$		
$\overline{oldsymbol{\Gamma}_{1v}}$	-12.71	-12.69	-12.64 (-12.62)	-12.69		-13.21	
$oldsymbol{\Gamma}_{15v}$	0.00	0.00	0.00 (0.00)	0.00	0.0	0.00	
$\boldsymbol{\Gamma}_{1c}$	0.38	0.57	1.09 (1.29)	1.32	1.02, (1.42)	1.5	
$oldsymbol{\Gamma}_{15c}$	3.74	3.73	$4.30 \ (4.46)$	4.60		4.61	
\mathbf{X}_{1v}	-10.37	-10.37	-10.23 (-10.38)	-10.27		-10.86	
\mathbf{X}_{3v}	-6.81	-6.79	-7.10 (-7.22)	-7.16		-6.81	
\mathbf{X}_{5v}	-2.59	-2.56	-2.79 (-2.83)	-2.71		-2.91	
\mathbf{X}_{1c}	1.29	1.80	$1.64 \ (1.75)$	2.65	2.07, (1.95)	1.90	
\mathbf{X}_{3c}	1.53	1.85	1.98 (2.09)	2.72		2.47	
\mathbf{X}_{5c}	10.20	10.33	10.88 (10.95)	11.20			
_	44.00	44.00	10.00 (11.00)	44.00		44.05	
\mathbf{L}_{1v}	-11.09	-11.08	-10.99 (-11.08)	-11.02		-11.35	
\mathbf{L}_{1v}	-6.61	-6.59	-6.91 (-6.97)	-6.91		-6.81	
\mathbf{L}_{3v}	-1.08	-1.10	-1.17 (-1.22)	-1.17		-1.41	
\mathbf{L}_{1c}	0.89	1.13	$1.45 \ (1.57)$	1.92	1.55, (1.75)	1.74	
\mathbf{L}_{3c}	4.58	4.67	5.12 (5.25)	5.65		5.45^{d}	
\mathbf{L}_{1c}	7.65	8.88	8.13 (8.00)	9.92		8.6^{d}	
E_g	0.38	0.57	1.09 (1.29)	1.32	1.02, (1.42)	1.5	

 ${}^a\mathrm{Ref.}^{52},\,{}^b\mathrm{Ref.}^{51},\,{}^c\mathrm{Ref.}^{17},\,{}^d\mathrm{Ref.}^{53}$

TABLE VI. Quasiparticle energies of AlAs for several states (in eV). The calculation of the self-energy is performed using 10 special **k**-points, 200 bands and 283 reciprocal lattice vectors. The size of the polarizability matrix is 169×169 and the plasmon pole model of von der Linden and Horsch¹⁰ is used. Our results are compared with those of Godby et al⁷ (GS) obtained using the RPA dielectric function for the screening of the Coulomb interaction, and these of Shirley, Zhu, and Louie (SZL) using a plsmon-pole model. The Godby et al results include spin-orbit coupling and the lower energy of a spin orbit pair is shown between brackets. Here E_g is the minimum band

	LDA		GW ap	GW approximation		
	Present	GS^b	Present	GS^b	SZL^e	
$\overline{oldsymbol{\Gamma}_{1v}}$	-12.13		-12.01 (-11.99)			
Γ'_{15v}	0.00	0.00 (-0.28)	0.00 (0.00)	0.00 [-0.28]	0.00	0.00
$oldsymbol{\Gamma}_{1c}$	1.92	2.29	2.79(2.97)	3.26	2.75	3.11^{c}
$oldsymbol{\Gamma}_{15c}$	4.19	4.23	4.91 (5.07)	5.05		
\mathbf{X}_{1v}	-10.08		-9.90 (-9.88)			
\mathbf{X}_{3v}	-5.58		-5.94 (-5.93)			
\mathbf{X}_{5v}	-2.26	-2.21 (-2.36)	-2.46 (-2.45)	-2.34 [-2.49]		-2.30
\mathbf{X}_{1c}	1.21	1.28	1.73 (1.90)	2.09	2.09	2.24
\mathbf{X}_{3c}	2.12	2.14	2.75 (2.90)	2.99		
\mathbf{X}_{5c}	10.38		11.22 (11.36)	11.20		
\mathbf{L}_{1v}	-10.65		-10.50 (-10.48)			
\mathbf{L}_{1v}	-5.76		-6.14 (-6.12)			
\mathbf{L}_{3v}	-0.85	-0.80 (-1.00)	-0.93 (-0.92)	-0.88 [-1.08]		-1.31
\mathbf{L}_{1c}	2.00	2.13	2.73 (2.89)	3.03	2.81	$2.49^c, 2.54^d$
\mathbf{L}_{3c}	4.59	4.58	5.29 (5.45)	5.48		

\mathbf{L}_{1c}	7.62		8.19 (8.34)			
E_g	1.21	1.37	1.73 (1.90)	2.09	2.09	2.32
Γ direct gap	1.92	2.29	2.79 (2.97)	3.26	2.75	3.11^{c}
X direct gap	3.47	3.47	4.19(4.35)	4.41		4.54
L direct gap	2.85	2.93	3.66 (3.81)	3.91		3.90^{d}

 $[\]overline{{}^a\mathrm{Ref.}^{52}, {}^b\mathrm{Ref.}^7, {}^c\mathrm{Ref.}^{59}, {}^d\mathrm{Ref.}^{60}, {}^e\mathrm{Ref.}^{17}}$

TABLE VII. Quasiparticle energies of InP for several states (in eV). The calculation of the self-energy is performed using 10 special **k**-points, 200 bands and 331 reciprocal lattice vectors. The size of the polarizability matrix is 169×169 and the plasmon pole model of von der Linden and Horsch¹⁰ is used. Our results are compared with those of Hott¹⁴. Here E_g is the minimum band gap.

	LDA		GW approxim	Expt.a	
	Present	$(\mathrm{H})^b$	Present	$(\mathrm{H})^b$	
$\overline{oldsymbol{\Gamma}_{1v}}$	-11.22	-11.50	-11.20 (-11.18)	-11.75	-11.6
Γ'_{15v}	0.00	0.00	0.00 (0.00)	0.00	0.00
$\boldsymbol{\Gamma}_{1c}$	0.77	0.50	1.54 (1.70)	1.23	1.460^{c}
$oldsymbol{\Gamma}_{15c}$	4.37	4.21	5.10 (5.24)	5.17	5.00^{d}
\mathbf{X}_{1v}	-9.18	-9.29	-9.08 (-9.14)	-9.16	-9.24
\mathbf{X}_{3v}	-5.56	-5.94	-5.82 (-5.84)	-6.60	-5.93
\mathbf{X}_{5v}	-2.04	-2.34	-2.21 (-2.21)	-2.52	-2.40
\mathbf{X}_{1c}	1.66	1.64	2.13 (2.26)	2.60	2.42
\mathbf{X}_{3c}	2.28	2.10	2.90 (3.02)	2.63	2.92
\mathbf{X}_{5c}	9.39	9.45	$10.26 \ (10.35)$	10.94	
\mathbf{L}_{1v}	-9.78	-9.94	-9.71 (-9.74)	-9.97	-9.89
\mathbf{L}_{1v}	-5.48	-5.90	-5.77 (-5.77)	-6.56	-5.93
\mathbf{L}_{3v}	-0.81	-0.94	-0.87 (-0.88)	-0.94	-0.98
\mathbf{L}_{1c}	1.57	1.30	2.28 (2.41)	1.97	2.32
\mathbf{L}_{3c}	4.92	4.75	5.60 (5.72)	5.85	5.68
\mathbf{L}_{1c}	7.12	7.47	7.74 (7.86)	8.17	
E_g	0.77	0.50	1.54 (1.70)	1.23	1.460^{c}

 $[\]overline{{}^a\mathrm{Ref.}^{61}, {}^b\mathrm{Ref.}^{14}, {}^c\mathrm{Ref.}^8, {}^d\mathrm{Ref.}^{62}}$

TABLE VIII. Quasiparticle energies of Mg₂Si for several states (in eV). The calculation of the self-energy is performed using 2 special \mathbf{k} -points, 200 bands and 645 reciprocal lattice vectors. The size of the polarizability matrix is 113×113 and the plasmon pole model of von der Linden and Horsch¹⁰ is used. Here E_g is the minimum band gap.

	LDA GW approximatio		$\mathrm{Expt.}^a$
$\overline{\Gamma_{1v}}$	-9.19	-8.82	
Γ_{15v}	0.00	0.00	0.00
Γ_{1c}	1.55	2.15	2.1
Γ_{25c}'	2.41	2.84	
\mathbf{X}_{1v}	-7.17	-6.91	
\mathbf{X}'_{4v}	-4.46	-4.67	
\mathbf{X}_{5v}'	-1.99	-2.14	
\mathbf{X}_{3c}	0.12	0.45	
\mathbf{X}_{1c}	0.20	0.62	
\mathbf{L}_{1v}	-7.71	-7.45	
\mathbf{L}_{2v}'	-4.79	-5.02	
\mathbf{L}_{3v}'	-0.73	-0.78	
\mathbf{L}_{1c}	0.98	1.50	
\mathbf{L}_{3c}	2.44	2.84	
$\mathbf{L}_{3v}^{\prime} ightarrow \mathbf{L}_{3c}$	3.17	3.62	3.7
$\mathbf{X}_{5v}^{\prime} ightarrow \mathbf{X}_{1c}$	2.19	2.76	2.5
E_g	0.12	0.45	0.7-0.80

 $[\]overline{{}^a\mathrm{Ref.}^{63}}$

TABLE IX. Quasiparticle energies of C for several states (in eV). The calculation of the self-energy is performed using 10 special **k**-points, 200 bands and 387 reciprocal lattice vectors. The size of the polarizability matrix is 169×169 and the plasmon pole model of von der Linden and Horsch¹⁰ is used. Here E_g is the minimum band gap.

	LDA		GW ap	proximation		$\mathrm{Expt.}^a$
	Present	$(RKP)^b$	Present	$(RKP)^b$	$(\mathrm{HL})^c$	
$\overline{oldsymbol{\Gamma}_{1v}}$	-21.45	-21.35	-22.66 (-22.65)	-22.88	-23.0	$-24.2\pm1^d, -21\pm1^e$
Γ'_{25v}	0.00	0.00	0.00 (0.00)	0.00	0.0	0.00
$oldsymbol{\Gamma}_{15c}$	5.53	5.58	7.39 (7.51)	7.63	7.5	7.3
Γ_{2c}'	13.29	13.10	15.38 (15.50)	14.54	14.8	$15.3 {\pm} 0.5^e$
\mathbf{X}_{1v}	-12.68	-12.61	-13.58 (-13.56)	-13.80		
\mathbf{X}_{4v}	-6.30	-6.26	-6.72 (-6.71)	-6.69		
\mathbf{X}_{1c}	4.61	4.63	6.19 (6.32)	6.30		
\mathbf{X}_{4c}	16.80	16.91	19.26 (19.37)	19.50		
\mathbf{L}_{2v}'	-15.58	-15.51	-16.66 (-16.65)	-16.95	-17.3	$-15.2 {\pm} 0.3^e$
\mathbf{L}_{1v}	-13.40	-13.33	-14.20 (-14.19)	-14.27	-14.4	-12.8 ± 0.3^{e}
\mathbf{L}_{3v}'	-2.79	-2.78	-2.99 (-2.98)	-2.98		
\mathbf{L}_{1c}	8.38	8.39	10.36 (10.48)	10.23		
\mathbf{L}_{3c}	8.86	8.76	10.66 (10.77)	10.63		
\mathbf{L}_{2c}'	15.45	15.67	17.59 (17.71)	18.14	17.9	$20{\pm}1.5^{e}$
E_g	4.01	4.01	5.60 (5.73)	5.67	5.6	5.48

 $[\]overline{{}^a\mathrm{Ref.}^{52}, {}^b\mathrm{Ref.}^{51}, {}^c\mathrm{Ref.}^5, {}^d\mathrm{Ref.}^{64}, {}^e\mathrm{Ref.}^{65}}$

TABLE X. Quasiparticle energies of LiCl for several states (in eV). The calculation of the self-energy is performed using 10 special **k**-points, 200 bands and 331 reciprocal lattice vectors. The size of the polarizability matrix is 259×259 and the plasmon pole model of von der Linden and Horsch¹⁰ is used. Here E_g is the minimum band gap.

	LDA		GW approxim	$\mathrm{Expt.}^a$	
	Present	$(\mathrm{HL})^b$	Present	$(\mathrm{HL})^b$	
$\overline{\Gamma_{15v}}$	0.00	0.00	0.00 (0.00)	0.00	
$oldsymbol{\Gamma}_{1c}$	5.86	6.00	8.73 (8.78)	9.1	
Γ_{25c}'	11.54	11.8	14.75 (14.79)	14.91	
\mathbf{X}_{4v}'	-2.98	-3.0	-3.49 (-3.47)	-3.3	
\mathbf{X}_{5v}'	-1.13	-1.1	-1.34 (-1.33)	-1.3	
\mathbf{X}_{1c}	7.54	7.5	10.48 (10.52)	10.7	
\mathbf{X}_{3c}	7.89	8.2	10.77 (10.80)	11.6	
\mathbf{L}_{2v}'	-2.95	-2.9	-3.47 (-3.46)	-3.2	
\mathbf{L}_{3v}'	-0.28	-0.2	-0.32 (-0.31)	0.3	
\mathbf{L}_{1c}	6.50	6.4	9.33 (9.37)	9.7	
\mathbf{L}_{3c}	9.52	9.03	$12.55 \ (12.58)$	12.5	
E_g	5.86	6.00	8.73 (8.78)	9.1	9.4

 $[\]overline{{}^a\mathrm{Ref.}^{66}, {}^b\mathrm{Ref.}^5}$

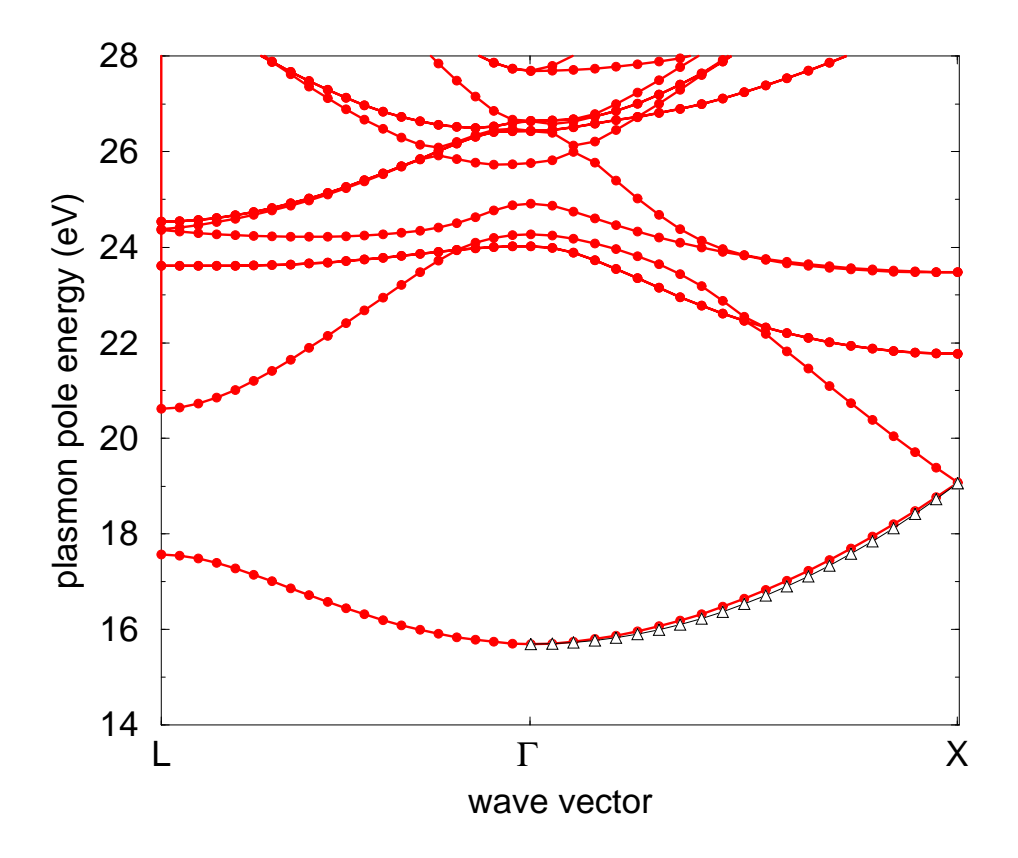
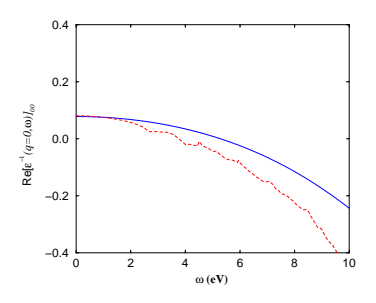


FIG. 1. Calculated Engel-Farid Plasmon model band structure of Si along L, Γ , and X high symmetry directions. The agreement with the results of Engel and Farid³⁶, and Aulbur⁴¹ are excellent. For small \mathbf{k} wave vectors the lowest plasmon band shows a quadratic dispersion (up-triangle curve) $\omega_0(\mathbf{k}) = \omega_0(\mathbf{0}) + \alpha |\mathbf{k}|^2$, with a dimensionless direction-dependent dispersion coefficient α . We find $\omega_0(\mathbf{0}) = 15.7$ eV and $\alpha_{\Delta} = 0.33$ in good agreement with the values of 15.91 eV and 0.34 of Engel and Farid³⁶ as well as the experimental values⁴² of 16.7 eV and 0.41.



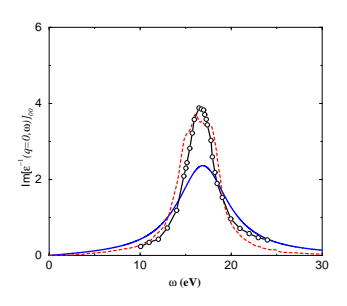


FIG. 2. Ab-initio calculated real and imaginary parts of the inverse dielectric function (dashed curve) of Si compared to the plasmon pole model of Hamada $et\ al$ (solid line) and with experiment (open circles)⁴².

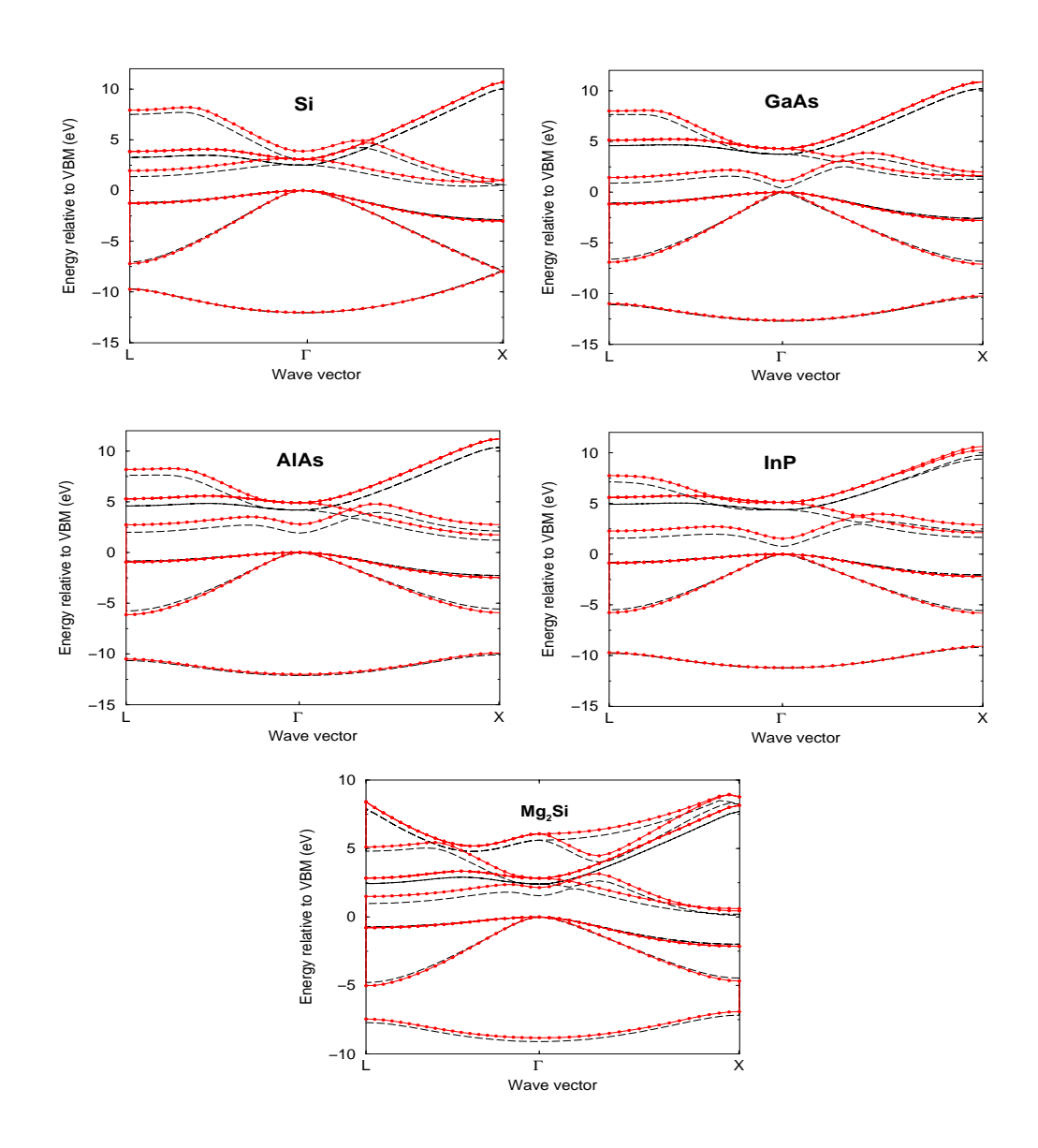


FIG. 3. Calculated electronic band structures along high symmetry directions for some small and medium band gap semiconductors: Si, GaAs, AlAs, InP, and SiMg₂ (in eV). The dashed lines display LDA results calculated with an energy cut-off of 15Ry (cf. Table IV,V,VI,VII, and VIII, column 2). The solid lines with dots show the GW results based on these LDA results (cf. Tables IV,V, VI,VII, and VIII, column 3). The energy scale is relative to the top of the valence state maximum (VBM).

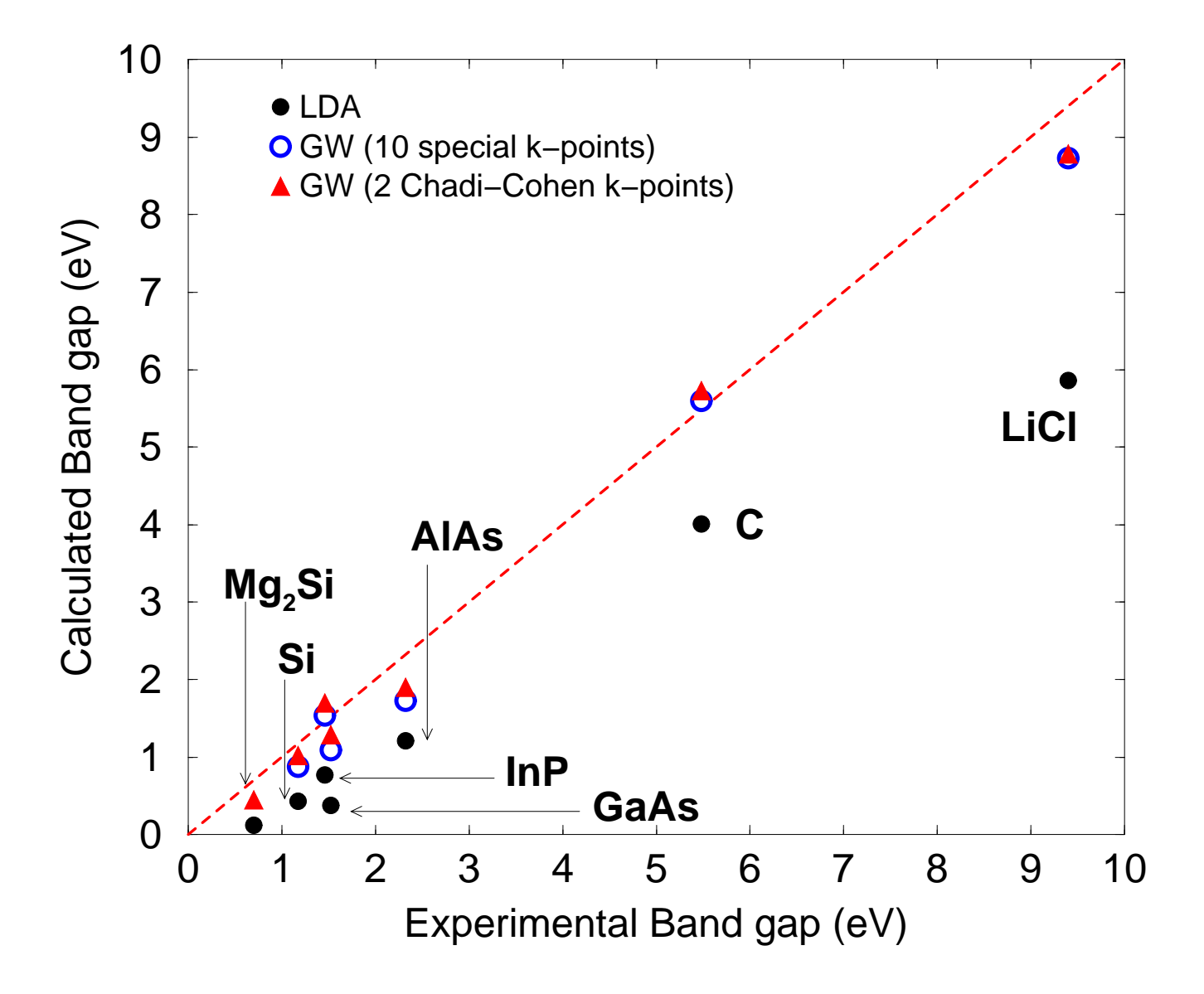


FIG. 4. Calculated LDA and GWA band gap compared to experimental results. The filled circles represent the LDA values, the open circles the GW values with 10 special **k**-points (corresponding to 256 points in the BZ) and the up-triangles the GW values using 2 chadi-Cohen **k**-points (corresponding to 32 points in the BZ). A perfect agreement with experiment is achieved when the calculated value is on the dashed line.

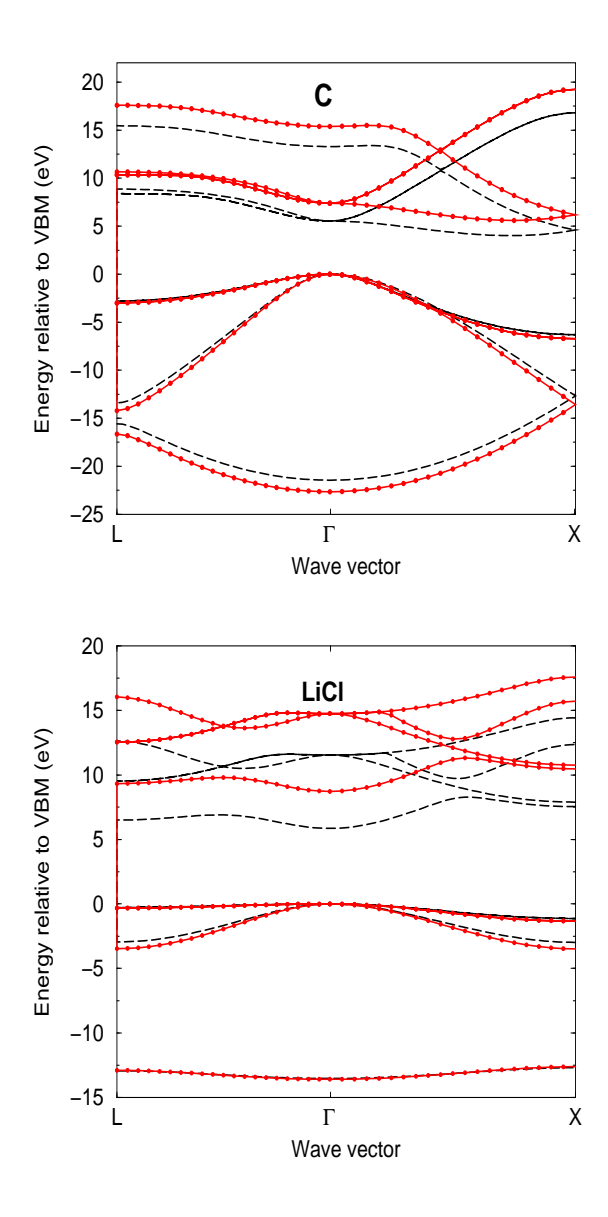


FIG. 5. Calculated electronic band structures along lines of high symmetry for some large band gap semiconductors: C, and LiCl (in eV). The dashed lines display LDA results calculated with an energy cut-off of 45Ry (cf. Table IX,X, column 2). The solid lines with dots show the GW results based on these LDA results (cf. Tables IX,X, column 3). The energy scale is relative to the top of the valence state maximum (VBM).

